ARISTOTLE UNIVERSITY OF THESSALONIKI
SCHOOL OF GEOLOGY
DEPARTMENT OF GEOLOGY
In collaboration with iPHEP, Universite de Poitier

KYNIGOPOULOU ZOI
Geologist

COMPARATIVE ANALYSIS OF OUTER AND INNER SKULL MORPHOLOGY BETWEEN *PARADOLICHOPITHECUS/PROCYNOCEPHALUS* AND CERCOPITHECINES.

MASTER THESIS

Thessaloniki

2017

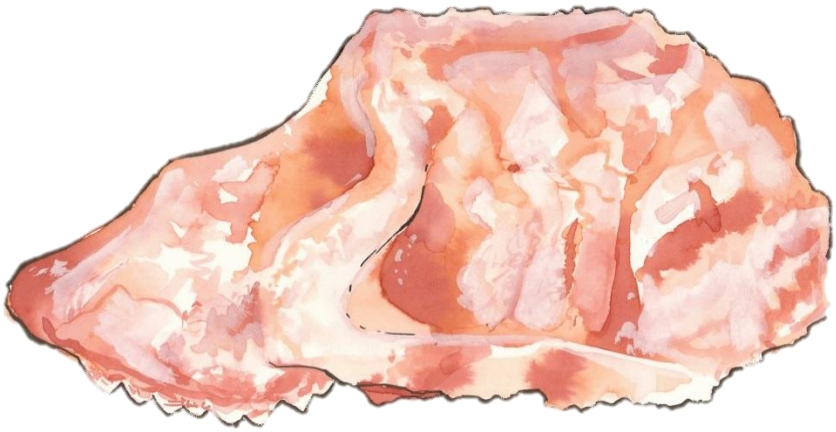

10mm

Ζωή Κ. Κυνηγοπούλου
Πτυχιούχος Γεωλόγος

ΣΥΓΚΡΙΤΙΚΗ ΑΝΑΛΥΣΗ ΤΗΣ ΕΞΩΤΕΡΙΚΗΣ ΚΑΙ ΕΣΩΤΕΡΙΚΗΣ ΚΡΑΝΙΑΚΗΣ ΜΟΡΦΟΛΟΓΙΑΣ ΑΝΑΜΕΣΑ ΣΤΟ ΓΕΝΟΣ PARADOLICHOPITHECUS/PROCYNOCEPHALUS ΚΑΙ ΤΟΥΣ ΚΕΡΚΟΠΙΘΗΚΙΔΕΣ.

Υποβλήθηκε στο Τμήμα Γεωλογίας στα πλαίσια του Μεταπτυχιακού Προγράμματος Εφαρμοσμένη και Περιβαλλοντική Γεωλογία
Τομέας Γεωλογίας
Αριστοτελείου Πανεπιστημίου Θεσσαλονίκης
Ημερομηνία Προφορικής Εξέτασης : 12 Μαΐου 2017

Τριμελής Εξεταστική Επιτροπή

Δημήτριος Σ. Κωστόπουλος, Αναπληρωτής Καθηγητής, Επιβλέπων Καθηγητής, ΑΠΘ
Γεώργιος Δ. Κουφός, Καθηγητής, Μέλος Τριμελούς Συμβουλευτικής Επιτροπής, ΑΠΘ
Franck Guy, Dr, Μέλος Τριμελούς Συμβουλευτικής Επιτροπής, University of Poitiers

Σχέδιο εξωφύλλου Παπανικολάου Χριστίνα.

Θεσσαλονίκη, Μάρτιος 2017

COMPARATIVE ANALYSIS OF OUTER AND INNER SKULL MORPHOLOGY BETWEEN *PARADOLICHOPITHECUS/PROCYNOCEPHALUS* AND CERCOPITHECINES.

ΣΥΓΚΡΙΤΙΚΗ ΑΝΑΛΥΣΗ ΤΗΣ ΕΞΩΤΕΡΙΚΗΣ ΚΑΙ ΕΣΩΤΕΡΙΚΗΣ ΚΡΑΝΙΑΚΗΣ ΜΟΡΦΟΛΟΓΙΑΣ ΑΝΑΜΕΣΑ ΣΤΟ ΓΕΝΟΣ PARADOLICHOPITHECUS/PROCYNOCEPHALUS ΚΑΙ ΤΟΥΣ ΚΕΡΚΟΠΙΘΗΚΙΔΕΣ.

Þar sem grær þar er von.
Allt sem græðir geymir von.
Úr klakaböndum kemur hún fram.
Af köldum himni fikrar sig fram.

to my sister

Contents

The present master thesis entitled ‘’Comparative analysis of outer and inner skull morphology between *Paradolichopithecus/Procynocephalus* and cercopithecines’’ has been written to fulfill the graduation requirements of the Master degree in Applied and Environmental Geology in the field of Structure and Evolution of Sedimentary Basins at the School of Geology of the Aristotle University of Thessaloniki (AUTH). The project was undertaken at the request of professor Dimitrios S. Kostopoulos and the research was done at the laboratory of Institut de Paléoprimatologie, Paléontologie, Humaine ; Evolution et Paléoenvironnements (iPHEP) at the University of Poitiers, France and the Laboratory of Geology and Palaeontology of the Aristotle University of Thessaloniki (LGPUT). The visit at Poitiers University was made possible thanks to the Erasmus + program.

The questions that this analysis raised were answered after conducting extensive investigation, while new hypothesis were also made. This wouldn’t have been achieved, had it not been for my supervisor prof. Dimitrios S. Kostopoulos, to whom I am grateful not only for the great opportunity, but also for his guidance and patience at all time. To this point I would also like to highly thank Dr Guy Franck and Dr Merceron Gildas of the iPHEP for their help and support, as well as all the people, colleagues, academic and technical support at the laboratory of Geology and Palaeontology at AUTH and iPHEP for the wonderful cooperation and in particular prof. George D. Koufos and Juliette Soubise. I am also grateful to the Digital Morphology Museum (DMM) of KUPRI that provides an open database of CT and MRI tomography scans of primates.

It would not have been possible to write this thesis without the help and support of all the kind people around me, yet only some of whom I can particularly name here. My parents and my sister have given me their full support and encouragement, for which the mere expression of thanks likewise does not suffice. I would also like to thank my friends Maria, Ruusi and especially my friend Christina for her exquisite drawings.

To all the readers, bear in mind Lord Byron’s quote ‘I deny nothing, but doubt everything’’

Zoi Kynigopoulou
Thessaloniki, March, 2017

CHAPTER 1. INTRODUCTION

The locality of Dafnero (sites: DFN1, DFN2 and DFN3) is located in Northern Greece close to the homonymous village of Kozani (Western Macedonia, Greece). The fossiliferous site of DFN1 was discovered in 1990 (Koufos *et al*., 1991) in the deep ravines of the eastern banks of Aliakmon River and bares Early Pleistocene (MN17) fossil mammals, i.e stenoid horses, cervids, bovids, giraffids, hyaenids, ursids, etc (Koufos, 2001; Kostopoulos *et al*., *submitted*). The other two fossiliferous sites DFN2 and DFN3 were discovered in 2010 during a Greek-French collaboration between the Laboratory of Geology and Paleontology of the Aristotle University of Thessaloniki, Greece and the Institut de Paléoprimatologie, Paléontologie, Humaine; 'Evolution et Paléoenvironnements (iPHEP, CNRS), Université de Poitiers, France.

Stratigraphically Dafnero consists of a 60m lithostratigraphic unit of thick terrestrial and fluvial sediments, which overlies uncomformably the mollasic sediments of the Tsotylion Formation of the Mesochelenic Trench (Fountoulis *et al*., 2001). Sites DFN1 and DFN3 belong to the same fossileferous layer of orange silty sands, which is placed half a meter bellow a thick (1-2m) conglomerate (Kostopoulos *et al*., *submitted*). The stratigraphic column and section of the site DFN3 are shown in Figure 1. Based on Koufos (2001) the fossil fauna of Dafnero-1, including *Nyctereutes megastoides*, *Equus stenonis* cf. *vireti*, *Eucladoceros senezensis* and more indicates an age between 2.4Ma and 1.8Ma.

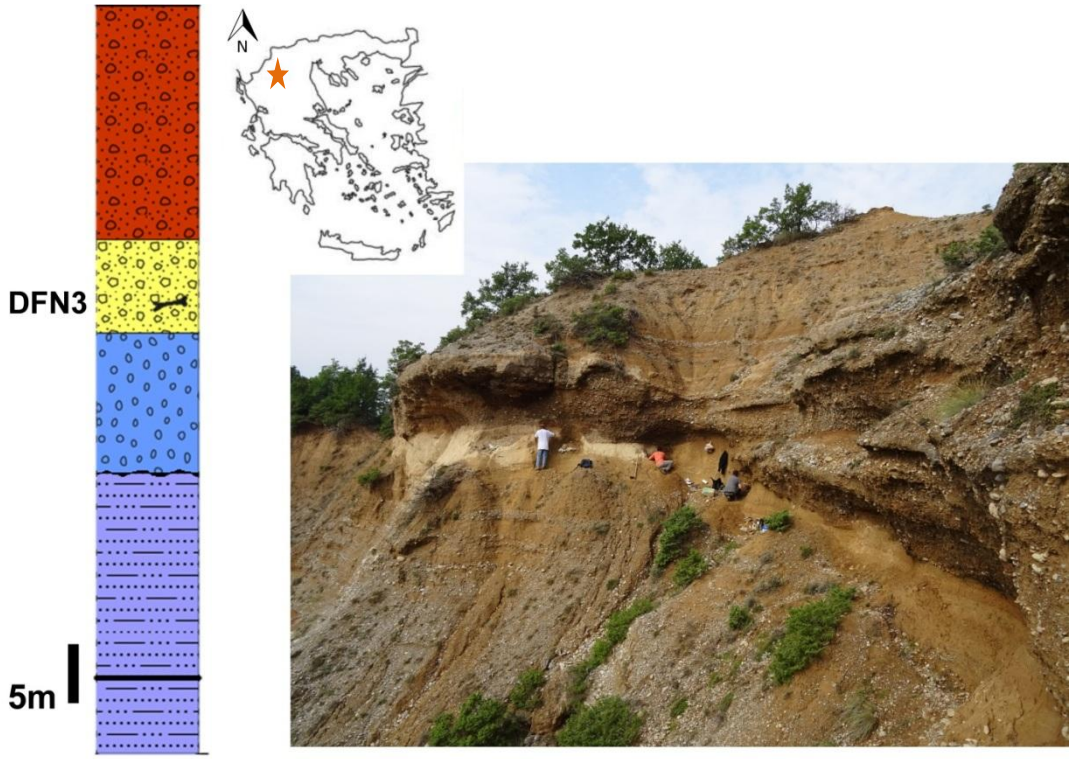

Figure 2: Stratigraphic settings, geographical position and image from the site of DFN3. Image provided by Kostopoulos D.S.

During field work of 2014, the cranium of a large-sized cercopithecid monkey, DFN3-150, was discovered in the DFN3 site. The cranium DFN3-150 is relatively well preserved; only a detachment along the skull's length results in the left side of the cranium slightly overlapping the right one. This suppression has deformed the left side partially and mainly in the facial area. The cranium bears also most of the upper dentition lacking the incisors and canines while the M^3's still erupting, identifying the DFN3-150 as a subadult individual. (Kostopoulos *et al*., *submitted*).

DFN3-150 has an elongated face with a smoothly elongated muzzle and long and narrow nasals; the interorbital distance is small, the neurocranium is long and the position of the inion is low. The upper dentition shows a strong protocone on P^3 and high crowned molars with strong flare (Kostopoulos *et al*., *submitted*). These features suggest that it belongs to the Cercopithecinae Subfamily (Delson and Nicolaescu-Plopsor, 1975; Delson, 1992; Szalay and Delson, 1979; Kostopoulos *et al.*, *submitted*). In addition with the lacrimal bone that expands anteriorly, the lacrimal fossa engulfed only in the lacrimal bone, the strongly elongated face, higher crowned molars with thick pronounced enamel, DFN3-150 belongs to the Papionini tribe (Delson and Nicolaescu-Plopsor, 1975; Delson, 1992; Szalay and Delson, 1979; Jablonski and Frost, 2010; Kostopoulos *et al*., *submitted*). Based on external and internal morphological traits Kostopoulos *et al.* (*submitted*) assigned DFN3-150 to *Procynocephalus*/*Paradolichopithecus* aff. *arvernensis*.

The Cerocopithecinae Subfamily of the Old Word monkeys consists of the tribes Papionini and Cercopithecini (Delson, 2000). During the Late Miocene in Africa the two subtribes Papionina and Macacina arose within the tribe of Papionini (Harris, 2000; Tosi *et al*., 2003; Raaum *et al*., 2005; Springer *et al*., 2012). The origin of the genus *Macaca* is dated at Late Miocene in Northern Africa (Delson, 1992) while during the latest Miocene (ca. 6-5.3 Ma) the genus invaded Europe and quickly dispersed into Eurasia; it is already present in China at the beginning of Pliocene (Rook *et al.*, 2001; Elton and O'Regan, 2014; Takai *et al.*, 2014; Alba *et al.*, 2014). Gilbert *et al*. (2014) hypothesized that the Late Miocene dispersal routes for the cercopithecoids, from Africa to Europe, were either over the Straits of Gibraltar / Mediterranean Basin or through the Arabian Sinai Penisula, whereas Takai *et al*. (2008) suggested that *Macaca* followed a northern dispersal route to inhabit eastern Eurasia during Pliocene and early Pleistocene. Today *Macaca* is the second most widely ranging primate, after *Homo.*

Instead, during the Plio-Pleistocene, Papionina diversified mainly in Africa leading into many genera adapted to different environments (Szalay and Delson, 1979; Jablonski, 2002; Gilbert, 2013; Nishimura *et al.*, 2014). The genus *Papio* is believed to originate from Southern Africa and quickly dispersed to the North and Western Africa (Kopp *et al.*, 2014). The Plio-Pleistocene Southern African species *P. izodi* and *P. angusticeps* were already similar to the extant small bodied papionins (Gilbert *et al*., 2014), whereas fossils at Olduvai Gorge, Absole and Bodo appear similar to modern *Papio hamadryas*; a taxon certainly occurring in the Middle Pleistocene but with molecular data dating its origin between 1.8 and 2.2 Ma in South Africa (Gilbert *et al.*,

2014). *Theropithecus* is considered to be an early Pleistocene African member of Papionina that invaded briefly Eurasia during late Early Pleistocene (Jablonski, 2002; Elton and O'Regan, 2014). Today only *P. hamadryas* is found outside Africa in Saudi Arabia and Yemen (Rowe, 1996).

Procynocephalus and *Paradolichopithecus* are considered as Pliocene to Pleistocene large representatives of fossil cercopithecines of Eurasia (Szalay and Delson, 1979; Jablonski, 2002; Kostopoulos *et al.*, *submitted*). The earliest occurrence of the genera is about 3.2 Ma in Central-Western Europe possibly corresponding to the first glacial climatic effects (Kostopoulos, *et al*., *submitted*), while during late Pliocene and early Pleistocene followed a northern route to inhabit Eastern Eurasia alongside *Macaca* (Takai *et al*., 2008). Early Pleistocene fossils ascribed to *P. arvernensis* Depéret, 1929 were found in Senèze, France (Depéret, 1929), Vialette, France (Heintz *et al*., 1974), La Puebla de Valverde, Spain (Heinz *et al*., 1971; Aguirre and Soto, 1978; Marigo *et al*., 2014), Vatera, Greece (de Vos *et al*., 2002), and recently in Dafnero, Greece (Kostopoulos *et al.*, *submitted*). *P. sushkini* Trofimov, 1977 is known from the site of Kuruksay, Tadjikistan (Trofimov 1977; Machenko 1994), and *P. gansuensis* Qiu, Deng, and Wang, 2004 from Longdan, Gansu, China (Qiu *et al.*, 2004), whereas *P. geticus* Necrasov, Samson, and Rădulesco, 1961 is described from Valea Graunceanului, Romania (Necrasov *et al*., 1961; Bolomey 1965). To the East, Late Pliocene/ Early Pleistocene fossils are referred to *Pr. wimani* Schlosser, 1924 from Xin'an, Henan, China (Schlosser, 1924) and *Pr. subhimalayanus* from India and China (von Meyer, 1848) (Table I in Appendix).

The taxonomic and phylogenetic position of *Paradolichopithesus* and *Procynocephalus* is controversial. Delson (1973) clearly placed *Paradolichopithesus* to the Cercobithecinae clade while many authors described the genus as a macaque with terrestrial and cranial similarities with open-woodlands baboons due to adaptation to similar ecological habitats (Jolly, 1967; Simons, 1970; Delson, 1973; Szalay and Delson, 1979; Delson, 2000, Groves, 2000, 2001; Jablonski, 2002; Frost *et al.*, 2005, Takai *et al.*, 2008, Nishimura *et al*., 2014, O'Shea *et al*., 2016). Maschenko (1994, 2005) and Takai *et al*. (2008) while studying *P. sushkini* stated that the genus should be placed closer to *Papio* showing a lacrimal fossa located only in the lacrimal bone, moderate maxillary and mandibular fossae and molars large relative to premolars. The genus *Procynocephalus* has a broad palate and molars with low and rounded cusps (Schlosser, 1924; Szalay and Delson, 1979; Jablonski, 2002) suggesting a closer affinity to macaques than baboons (Szalay and Delson, 1979; Jablonski, 2002). The two genera of *Paradolichopithesus* and *Procynocephalus* are regarded as closely related since they show similarities in the body mass and dental morphology (Delson and Nicolaescu-Plopsor, 1975; Szalay and Delson, 1979; Takai *et al*., 2008). These features as well as the same ecological habits (grasslands along same latitudes of Eurasia during Plio/Pleistocene) led Kostopoulos *et al*. (*submitted*) to account *Paradolichopithesus* as a synonym to *Procynocephalus*. The current study also considers them alike and uses the term *Procynocephalus*/ *Paradolichopithecus*.

A new method that is used in order to further study the specimens of *Procynocephalus*/ *Paradolichopithecus* is the inner morphologies of the cranium and particularly the maxillary sinuses (Nishimura *et al*., 2007, 2009, 2010, 2014). The maxillary sinus (MS) is an empty cavity of the rostrum located in the posterolateral region bilaterally of the nasal cavity (Figure 2). It is formed postnatally in the cancellous bone of the maxilla and it is connected with the middle meatus of the nasal cavity through a narrow ostium (Cave, 1967; Witmer, 1999; Weiglein, 1999; Maier, 2000; Rae and Koppe, 2003; Rossie, 2006; Nishimura *et al*., 2007; Ito *et al*., 2009). The maxillary sinuses were lost in the common ancestor of the extant cercopithecoids and reoccur only in macaques lineage within the Cercopithecinae (Rae *et al*., 2002; Rae, 2008; Nishimura and Ito, 2014), while baboons were thought to have negligible cancellous maxillary body (Koppe and Ohkawa, 1999; Rae and Koppe, 2000; Nishimura *et al*., 2005; Nishimura *et al*., 2009). However, MS has been found in specimens of Papionina such as *Papio* and *Theropithecus* (Nishimura *et al*., 2014). The volume/size of the MS has also been studied and many species of macaques were categorized based on that (Ito and Nishimura, 2016). Nowadays, the presence and size of the MS is considered a dubious phylogenetic factor.

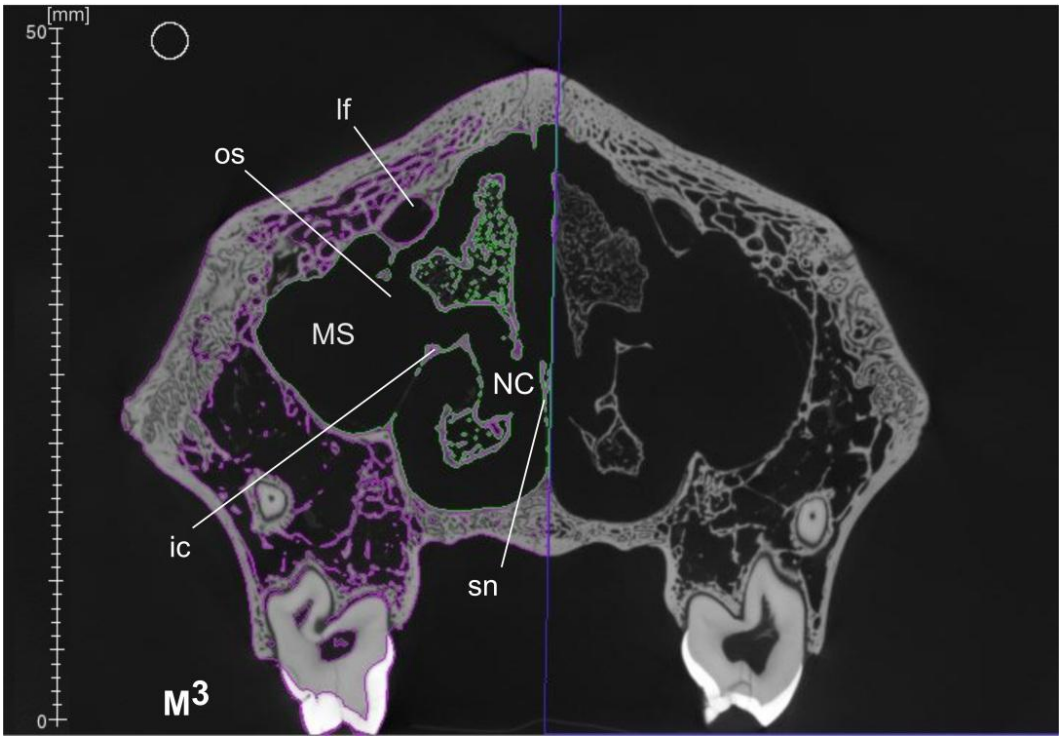

Figure 2. Coronal microCT scanning image of a male specimen *Macaca sylvanus* cranium (id: I, scanned by iPHEP, University of Poitiers) at the level of M^3 during its process with the Avizo software with the left side being highlighted since it was the one studied. The nasal cavity (NC) is divided by the septum nasi (sn). The inferior concha (ic) and the lacrimal fossa (lf) are distinguished and also the position of the ostium (os) that connects the nasal cavity (NC) with the maxillary sinus (MS) is estimated.

The present study focuses on the external morphometrical distances of the fossil cranium of *Procynocephalus*/ *Paradolichopithecus* aff. *arvernensis* DFN3-150. Craniums of extant species of *Macaca* and *Papio* were used as comparative material. Kostopoulos *et al*. (*submitted*) described the fossil cranium and found that it shares a combination of features of both *Papio* and *Macaca*. The orbital part of the zygomatic bone, the interorbital distance, the elongated face and muzzle along with the engulfed lacrimal fossa are baboon like features. On the other hand, there is no maxillary fossa but it has maxillary sinuses and a squarish basioccipital bone as macaques. The fossil cranium has also maxillary sinuses and thus the morphology and size of the MS were further studied. The ultimate aim of the study is to investigate in more detail the affinities of the DFN3-150 cranium with either *Papio* or *Macaca* based on the external and inner cranial morphological features and also to test the phylogenetic value of the MS's presence, size and shape. Considering the geographical distribution and the existing studies on the three taxa *Macaca*, *Papio* and *Procynocephalus*/*Paradolichopithecus* hypotheses on the phylogenetic correlation were also proposed.

Figure 3. Image of the studied cranium DFN3-150 in situ at Dafnero 3 site from Kostopoulos *et al*., *submitted.*

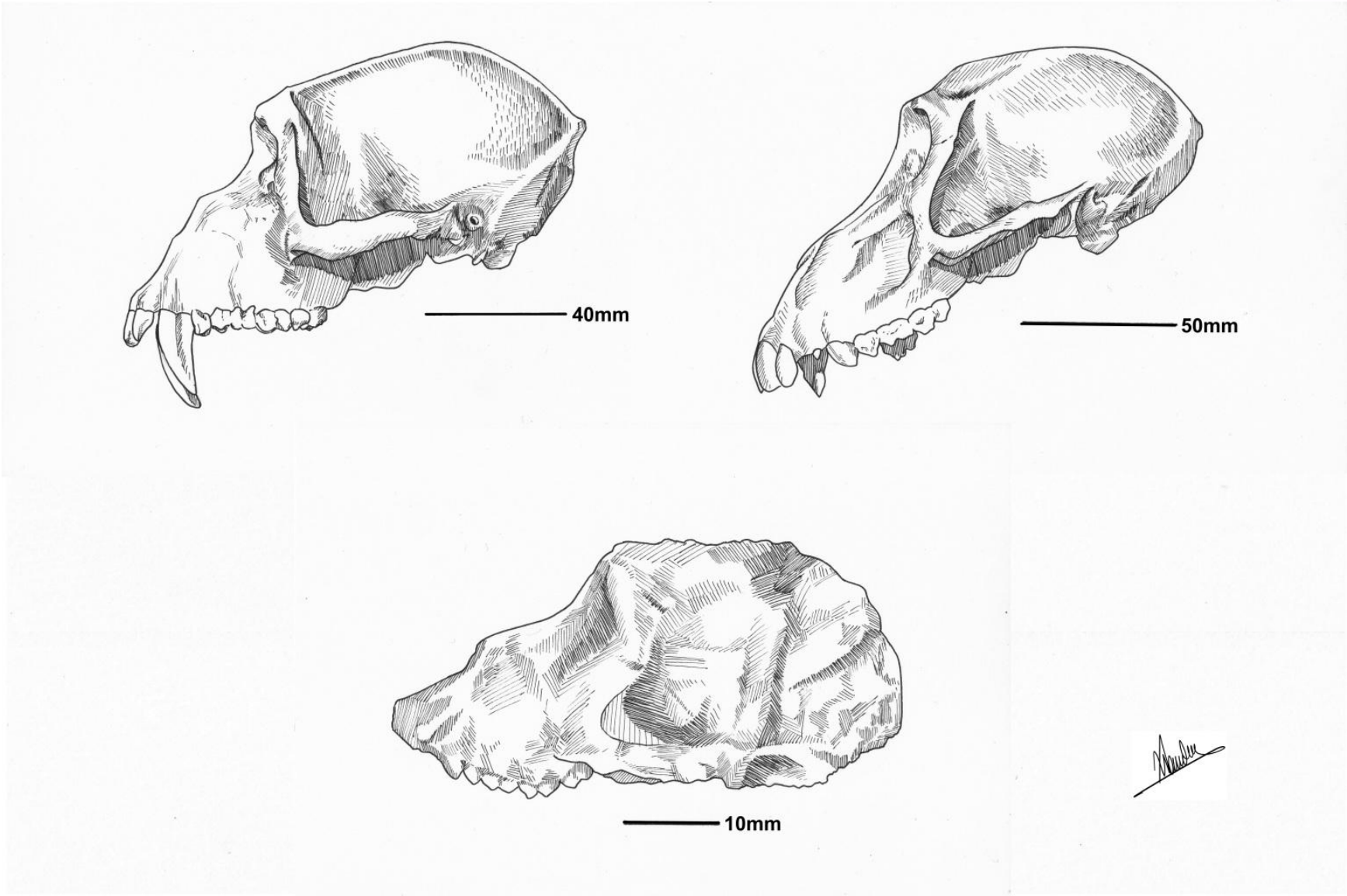

Figure 4. Drawing sketches of *Macaca sylvanus* (top left), *Papio anubis* (top right) and the fossilized cranium DFN3-150 of *Procynocephalus*/ *Paradolichopithecus* aff. *arvernensis*. Artist Papanikolaou Christina.

CHAPTER 2. MATERIALS AND METHODS

Since *Procynocephalus/Paradolichopithecus* is recognized as a member of Papionini, the cranial comparison is focused on representatives of the two closely related extant genera, which are *Papio* and *Macaca* (Jablonski, 2002; Rae, 2008). Craniums of three species of *Papio*, i.e. *Papio anubis*, *Papio hamadryas* and *Papio ursinus*, and four species of *Macaca*, i.e. *Macaca sylvanus*, *Macaca nemestrina*, *Macaca silenus* and *Macaca fascicularis* were used as comparative material. Taxa selection was based principally on similarities in size with the fossil species, as well as on geographic distribution. The geographical distribution can provide additional information in taxonomical correlations between the fossil and the comparative taxa, but it is also very important in the study of maxillary sinuses (MS), as it is believed that changes in size and shape of the maxillary sinuses response to changes in the nasal cavity (NC) under climatic pressure (Ito *et al*., 2014b).

Fossils from baboon-like species are dated back to 2.5 Ma and disperse mostly in South Africa during Plio-Pleistocene (Delson, 1992). The macaques first appeared in the late Miocene in North Africa, while from the earliest Pliocene to the last interglacial they inhabited Europe (Elton and O'Regan, 2014). Fossils from India show that macaques spread in Asia around 3 Ma, while teeth from China are dated back to even 5 Ma ago (Delson, 1992). Takai *et al.* (2008) also hypothesized a northern Central Eurasian route of migration to Asia for the large cercopithecine *Procynocephalus/Paradolichopithecus*.

Today, *Papio* can be found mostly in the African and Arabian areas in small range of latitude (Rowe, 1996), while *Macaca* species are mainly located in Asia except *M. sylvanus*, a species restricted today in Morocco, Africa. Moreover, macaques are found in a wide range of latitude, making them able to live in a wide variety of climates and habitats than any other primate, except humans (Rowe, 1996). To eliminate these differences, the selected species of the two genera can be found in approximately similar latitudes and relatively nearby areas (Table 1).

Table 1. Comparative sample of the extant species. Data on weight and geographical range are from Rowe (1996).

Species	Number of specimens	Average weight ♂ (kg)	Areas
Papio anubis	6	28.4	Equatorial Africa
Papio hamadryas	4	21.3	Somalia, Ethiopia, Saudi Arabia, Yemen
Papio ursinus	1	20.4	Southern Africa
Macaca sylvanus	5	15.3-17	Morocco, Algeria, Gibraltar
Macaca nemestrina	4	6.2-14.5	Burma to Malay Peninsula, Sumatra
Macaca silenus	2	5-10	West India
Macaca fascicularis	2	4.7-8.3	Southern Indochina, Burma, Indonesia, Philippines, Nicobar Islands

A total number of 24 extant craniums was studied, two of which were original/natural craniums while the rest 22 were the 3D images produced from either CT or microCT scanning of original craniums. The two original craniums (*Macaca sylvanus* I, *Papio anubis* C2) are housed at the Institut de Paléoprimatologie, Paléontologie, Humaine; 'Evolution et Paléoenvironnements (iPHEP), Université de Poitiers. The fossil cranium of *Procynocephalus/Paradolichopithecus* (DFN3-150) is housed in the Laboratory of Geology and Paleontology of the University of Thessaloniki (Table 2).

The 3D images of the craniums used in this study were provided by the institute of iPHEP and the Digital Morphology Museum (DMM) of KUPRI (http://dmm3.pri.kyoto-u.ac.jp/dmm/WebGallery/index.html), Primate Research Institute of Kyoto University. In order to study the maxillary sinuses in all of our specimens, the original craniums of the extant species as well as the fossil one from Dafnero 3 were also scanned in iPHEP.

Table 2. Information for each specimen regarding the sex, the code and the institution they are being housed at.

Species	Sex	Code	Institution	Subject ID
Procynocephalus aff. arvernensis	Female **juv**	DFN3 150	Laboratory of Geology and Paleontology of the University of Thessaloniki	DFN3-150
Macaca sylvanus	Male	I	iPHEP, University of Poitiers	I
Macaca sylvanus	Male	PRICT-1152KUPRI	Japan Monkey Centre	1392
Macaca sylvanus	Female	PRICT-1136 KUPRI	Japan Monkey Centre	3741
Macaca sylvanus	Male	PRICT-1122 KUPRI	Japan Monkey Centre	5155
Macaca sylvanus	Female	PRICT-1483 KUPRI	Primate Research Institute, Kyoto University	7114
Macaca nemestrina	Female	PRICT-1470 KUPRI	Primate Research Institute, Kyoto University	3647
Macaca nemestrina	Female	PRICT-1469 KUPRI	Primate Research Institute, Kyoto University	3054
Macaca nemestrina	Male	PRICT-1441 KUPRI	Department of Anatomy (Macro), Dokkyo Medical University	1104
Macaca nemestrina	Male	PRICT-1108 KUPRI	Primate Research Institute, Kyoto University	2454
Macaca silenus	Female	PRICT-38 KUPRI	Primate Research Institute, Kyoto University	7114
Macaca silenus	Male	PRICT-726 KUPRI	Primate Research Institute, Kyoto University	8138
Macaca fascicularis	Male	PRICT-1157 KUPRI	Department of Anatomy (Macro), Dokkyo Medical University	995
Macaca fascicularis	Female	PRICT-713 KUPRI	Primate Research Institute, Kyoto University	1400
Papio anubis	Male **juv**	80-44-M-101	Royal Museum of Central Africa, Tervuren, Belgium	80-44-M-101
Papio anubis sp.	Male **juv**	C2	iPHEP, University of Poitiers	C2
Papio anubis	Female **juv**	PRICT-733 KUPRI	Primate Research Institute, Kyoto University	3086
Papio anubis	Male	PRICT-351 KUPRI	Primate Research Institute, Kyoto University	1626

Papio anubis	Male	960_H60s	Royal Museum of Central Africa, Tervuren, Belgium	960_H60s
Papio anubis	Female	90042M228	Royal Museum of Central Africa, Tervuren, Belgium	90042M228
Papio ursinus	Male	PRICT-734 KUPRI	Primate Research Institute, Kyoto University	5799
Papio hamadryas	Female	PRICT-93 KUPRI	Primate Research Institute, Kyoto University	3390
Papio hamadryas	Male	PRICT-404 KUPRI	Primate Research Institute, Kyoto University	5341
Papio hamadryas	Male	PRICT-417 KUPRI	Primate Research Institute, Kyoto University	6077
Papio hamadryas	Female	PRICT-424 KUPRI	Primate Research Institute, Kyoto University	3390

CT and microCT scanning

CT scan (computed tomography) is a process that has being long ago introduced in Paleontology but the recently and more developed microCT scan has been proved very efficient in modern studies. Many applications of microCT scan help in 3D studies of paleontological specimens. These applications have two major advantages; they are based on nondestructive procedures and can reveal both the outer and the inner structures of the scanned fossils. In anthropology and primatology microCT scan is also very useful and has recently been used in the study of the dentine and the enamel of the teeth. Suwa *et al*. (2007) analyzed the dentino-enamel junction (DEJ) in the gorilla clade, while high spatial resolution was used to study the dentine, enamel, and DEJ of *Homo neanderthalensis* (Macchiarelli *et al*., 2006) and early *Homo sapiens* (Smith *et al*., 2007). With microCT scan the endocranium volume (Simons *et al*., 2007) as well as inner structures of primate crania has also been investigated.

The process of CT scan uses X-ray images to produce three dimensional representations of a scanned object. There are three phases to produce CT images, while the factors associated in each phase can affect the characteristics and quality of the images. The first phase is scanning during which a source sends a beam of X-rays that passes through the object. The amount of radiation that penetrates the object is later recorded by the detector (scan data) (Smith, 1999). There are two types of set ups for scanning. In the first one, the X-ray source and detector are stationary and the object is rotating. In the second set up, the object is still while the source and detector are rotating around it (Ritman, 2004).

The second phase is the image reconstruction process in which the scan data is processed and a digital image (a matrix of pixels) is produced. During this phase the digital image processing algorithms are settled (filtered back projection algorithm). That way the quality of the images and the details are improved, while the noise is minimized (Stock, 2009). Micro-CT scan follows the same principals with CT scan but with microscopic details and the pixel size of the produced images is in micrometer range (Dame *et al*., 2006).

Finally, the digital images are converted into visible analog images while the main principal is the density of the object. Materials like bones and teeth block more X-rays resulting in low signal (Smith, 1999). As a result, different shades of gray or different brightness levels are used to indicate different density/signal. The factors that control this process (windowing and width control) are adjustable (Stock, 2009). In general, CT has very high contrast sensitivity and even small differences in density can be visible. Thus even the cancelous bones can be distinguished from the bones, which is very useful in the present study because even the slightest pneumatization of the maxilla can be detected.

3D images provided by iPHEP were produced with EasyTom XL Duo µCT 110 at Centre 113 de Microtomographie (IC2MP, iPHEP, Université de Poitiers). The X-ray source is a sealed Hamamatsu microfocus x-ray source - 75W, 150 kV. The detector is an 111 amorphous silicon based detector Varian PaxScan 2520DX - 1536x1920 pixel matrix; 112 127µm pixel pitch, 16 bits, CsI conversion screen. Each specimen that was scanned in iPHEP was securely packed to reassure its stability in the chamber (Fig 5). The 3D images that were downloaded for free from the DMM of KUPRI were produced by CT scanning (http://dmm3.pri.kyoto-u.ac.jp/dmm/WebGallery/index.html) . More details regarding the scanning Institution and the resolution of the 3D images of each the specimens are given in Table 3.

Table 3. Information for the 3D scanned images of each specimen.

Species	Code	Scanning institution	Resolution	Slices	Citation
Procynocephalus aff. arvernensis	DFN3 150	iPHEP	0.0699(mm)*0.0699(mm)	1771	Kostopoulos *et al*., 2016?
Macaca sylvanus	I	iPHEP	0.0536(mm)*0.0536(mm)	1784	Kostopoulos *et al*., 2016?
Macaca sylvanus	PRICT-1152KUPRI	Primate Research Institute, Kyoto University	0.277 (mm)*0.277 (mm)	508	
Macaca sylvanus	PRICT-1136 KUPRI	Primate Research Institute, Kyoto University	0.254 (mm)*0.254 (mm)	398	
Macaca sylvanus	PRICT-1122 KUPRI	Primate Research Institute, Kyoto University	0.282 (mm)*0.282 (mm)	483	Ito *et al*., 2014a
Macaca sylvanus	PRICT-1483 KUPRI	Primate Research Institute, Kyoto University	0.230 (mm)*0.230 (mm)	508	
Macaca nemestrina	PRICT-1470 KUPRI	Primate Research Institute, Kyoto University	0.181 (mm)*0.181 (mm)	670	
Macaca nemestrina	PRICT-1469 KUPRI	Primate Research Institute, Kyoto University	0.156 (mm)*0.156 (mm)	587	
Macaca nemestrina	PRICT-1441 KUPRI	Primate Research Institute, Kyoto University	0.263 (mm)*0.263 (mm)	500	
Macaca nemestrina	PRICT-1108 KUPRI	Laboratory of Physical Anthropology, Kyoto University	0.199 (mm)*0.199 (mm)	663	Ito *et al*., 2014a
Macaca silenus	PRICT-38 KUPRI	Primate Research Institute, Kyoto University	0.250 (mm)*0.250 (mm)	508	Nishimura *et al*., 2014
Macaca silenus	PRICT-726 KUPRI	Primate Research Institute, Kyoto University	0.313 (mm)*0.313 (mm)	391	Nishimura *et al*., 2014

Maca fascicularis	PRICT-1157 KUPRI	Primate Research Institute, Kyoto University	0.244 (mm)*0.244 (mm)	438	Ito *et al*., 2014a
Macaca fascicularis	PRICT-713 KUPRI	Primate Research Institute, Kyoto University	0.200 (mm)*0.200 (mm)	640	Nishimura *et al*., 2014
Papio anubis	80-44-M-101	iPHEP	0.054(mm)*0.054(mm)	1784	Kostopoulos *et al*., 2016?
Papio anubis sp.	C2	iPHEP	0.0829(mm)*0.0829(mm)	2189	
Papio anubis	PRICT-733 KUPRI	Primate Research Institute, Kyoto University	0.375 (mm)*0.375 (mm)	436	Nishimura *et al*., 2014
Papio anubis	PRICT-351 KUPRI	Primate Research Institute, Kyoto University	0.468 (mm)*0.468 (mm)	282	Nishimura *et al*., 2014
Papio anubis	960_H60s	University Hospital, UZ Leuven	0.489(mm)*0.489(mm)	595	
Papio anubis	90042M228	University Hospital, UZ Leuven	0.391(mm)*0.391(mm)	638	
Papio ursinus	PRICT-734 KUPRI	Primate Research Institute, Kyoto University	0.468 (mm)*0.468 (mm)	515	Nishimura *et al*., 2014
Papio hamadryas	PRICT-93 KUPRI	Primate Research Institute, Kyoto University	0.214 (mm)*0.214 (mm)	1780	
Papio hamadryas	PRICT-404 KUPRI	Primate Research Institute, Kyoto University	0.300 (mm)*0.300 (mm)	1076	Nishimura *et al*., 2014
Papio hamadryas	PRICT-417 KUPRI	Primate Research Institute, Kyoto University	0.300 (mm)*0.300 (mm)	1056	Nishimura *et al*., 2014
Papio hamadryas	PRICT-424 KUPRI	Primate Research Institute, Kyoto University	0.250 (mm)*0.250 (mm)	861	Nishimura *et al*., 2014

Figure 5. On the left, the scanning chamber with the detector monitor, the scanning skull *P. anubis* C2 and the X-ray source. On the right, the microCT scan EasyTom XL Duo at Centre 113 de Microtomographie (IC2MP, iPHEP, Université de Poitiers).

Figure 6. The fossil cranium of *Procynocephalus/Paradolichopithecus* DFN3-150 found in Dafnero 3, northern Greece. Lateral view of the original on the left and the lateral view of the 3D images produced by microCT scanning at IC2MP, iPHEP, Université de Poitiers on the right. Scale bar: 10mm.

External Measurements

The two comparative taxa of *Papio* and *Macaca* show many differences in the external features of their craniums. In *Papio* the muzzle is longer relative to the neurocranium, with distinctive maxillary and mandibular fossae (Strasser and Delson, 1987). The anterorbital concavity is steeper in *Papio* and the lacrimal fossa is in the lacrimal bone. In all *Macaca* species the lacrimal fossa is in the lacrimal bone but in contact with the frontal process of the maxilla (Nishimura *et al*., 2007; Takai *et al*., 2008). As a result the craniums of the extant species of *Procynocephalus/Paradolichopithecus* were studied based on these main differences.

Twenty-eight metrical data were taken using common landmarks (Figure 5). All measurements are in mm (Table 4) and include basic dimensions of the whole cranium, such as the basicranial length, the skull length, the cranial length and height, the facial length and the upper facial length. Moreover, the basic dimensions of the orbits as well as of the foramen magnum were measured. Because the muzzle shows many differences between *Papio* and *Macaca*, the placements and distances of nasion, rhinion, nasospinale, prosthion and staphylion were measured more extensively. The maxillary sinuses' development takes place in the body of the maxilla, along the palatal bone and is parallel to the nasal cavity, so many measurements were focused in these areas too. All the measurements were done with a caliper for the two original/natural craniums and the fossil, while the 3D images of the rest of the craniums were measured using Avizo software measuring tool.

Table 4. Basic external cranial measurements and the landmarks used in this study.

Measurements	Landmarks	Code
Basicranial length	basion-nasion	ba_n
Skull length	inion-prosthion	i_pr
Cranial length	inion-nasion	i_n
Facial length	basion-prosthion	ba_pr
Cranial base length	basion-staphylion	ba_sta
Cranial height	basion-bregma	ba_b
Upper Facial height	prosthion-nasion	pr_n
Biporionic breadth	porion-porion	po_po
Foramen Magnum maximum width	posterior edges of the occipital condyles	FM_width
Foramen Magnum maximum length	basion-opisthion	FM_length
Position Foramen Magnum end	opisthion-staphylion	o_sta
Prosthion placement	prosthion-porion	pr_po
Nasion placement	porion-nasion	po_n
Palatal length	staphylion-prosthion	sta_pr
Bicanine breadth	P^3-C	Prem_Cani
Bimolar breadth	M^1-M^2	M1_M2
Middle M^3 breadth	M^3-M^3	M3_mid
Nasal height	nasion-nasospinale	n_ns
Nasal length	nasion-rhinion	n_rhi
Biorbital breadth	frontomalare temporale-frontomalare temporale	fmt_fmt
Postorbital min breadth	pterion-pterion	pt_pt
Glabela placement	porion-glabela	po_g
Average Orbits width	dacryon-frontomalare orbitale	Orbits_width
Average Orbits height	zygomax superior-midtorus inferior	Orbits_height
Inion placement	inion-opisthion inion-bregma	o_i b_i
Bregma placement	bregma-opisthion	b_o
Distance between Carotid Canal of Foramen	middle of carotid canal – middle of carotid canal	Carotid_Foramen_distance

Table 5. List of landmarks used in present study and their description.

Number	Points	Description
1	prosthion	most anterior point in the midline on the alveolar process of the maxilla
2	nasospinale	most inferior midline point of piriform aperture
3	rhinion	most anterior point in midline on the nasal
4	nasion	middle of fronto-nasal suture
5	glabella	most anterior point of the frontal
6	frontomalare temporale	crossing point of frontozygomatic suture and lateral edge of zygoma
7	frontomalare orbitale	crossing point of frontozygomatic suture and the inner orbital rim
8	dacryon	junction of frontal, lacrimal and maxilla
9	zygo-max superior	superior point of zygomaxillary suture
10	mid-torus inferior	inferior margin of superaorbital torus
11	inion	most prominent projection of the protuberance
12	opistion	most posterior point of foramen magnum
13	basion	most anterior point of foramen magnum
14	posterior occipital condyles	most posterior edge of occipital condyles
15	middle of carotid canal	middle of the carotid passageway in the temporal bone
16	porion	upper margin of auditory meatus
17	staphylion	midpoint of the posterior edge of the hard palate
18	M^2-M^3 contact	on buccal self
19	M^1-M^2 contact	on buccal self
20	P^3-C contact	on buccal self
21	bregma	point where the coronal suture is intersected by the sagittal suture
22	pterion	region where the frontal, parietal, temporal and sphenoid join

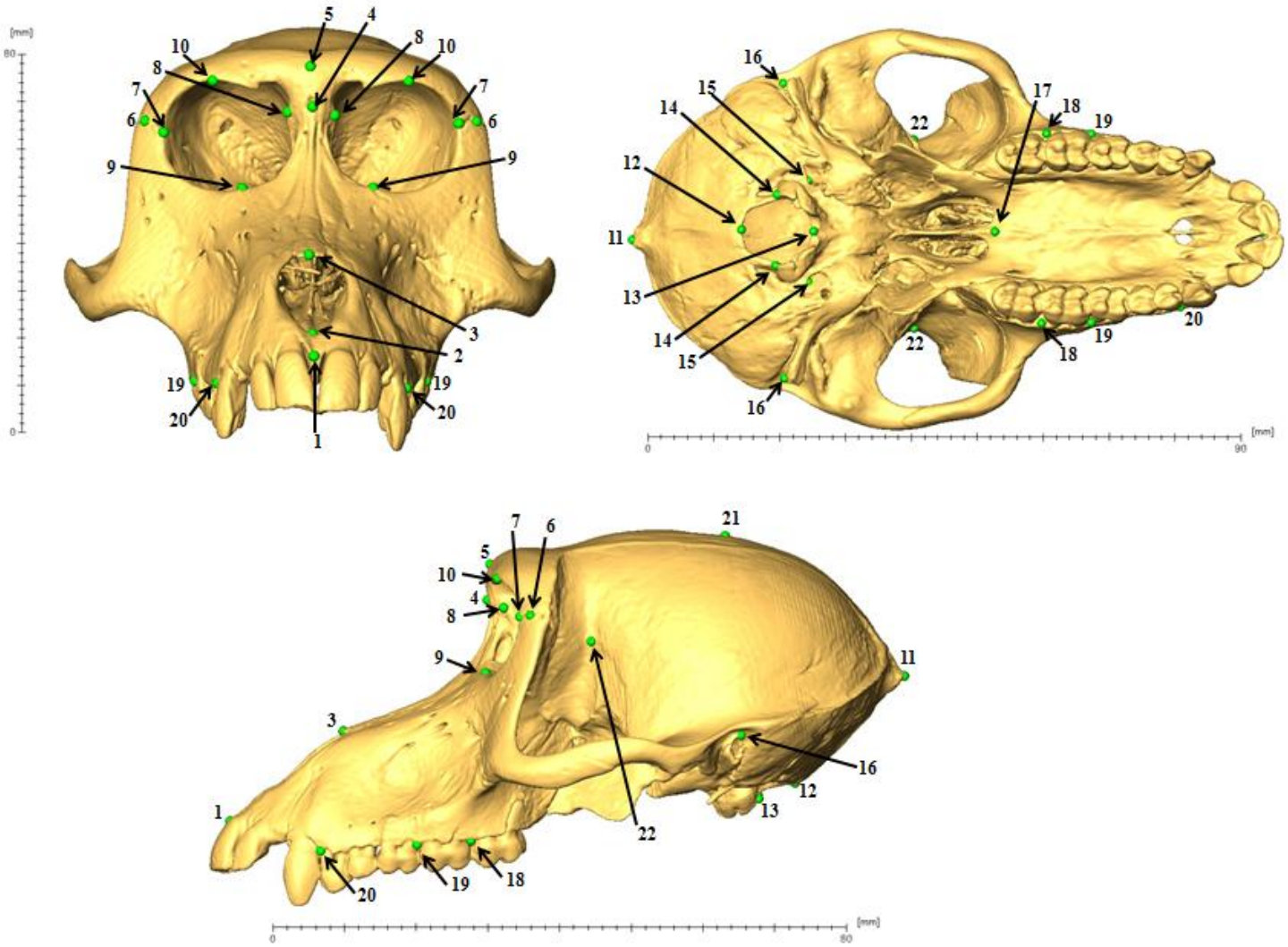

Figure 7. The 22 landmarks used for the metrical distances measured in this study. Each landmark is explained in Table 5. The images were taken while measuring *P. hamadryas* PRICT-424 KUPRI in Avizo software.

Apart from the metrical data, some angles were also calculated for each specimen using Avizo tools (Table 6). The Flower angle refers to the angle that is formed between the prostion-basion-nasion landmarks and represents the lower part of the muzzle. The displacement of the middle muzzle area was measured by the Middle Muzzle angle between basion, rhinion and nasion landmarks. Additionally, some angles were calculated to estimate the position of orbital plane (Orbital plane^Frankfurt's plane) and the placement of the inion (Occipital plane^Frankfurt's plane). In order to measure the latter two angles, the two relevant planes for each angle were set using the Avizo software tool ''Ortho Slice''. Each plane was set according to landmarks and then the angle formed between the two planes was measured. The Frankfurt's plane was used for both angles and was placed using the two porion landmarks and the inferior margin of the left orbit. To estimate the position of the orbital

plane, the Frankfurt's plane and the orbital plane were used; the latter was placed using the inferior margin of each orbit and the superior margin of the left orbit. For the position of the inion, the Frankfurt's plane and the occipital plane were used, whereas the latter plane was placed using the inion and the posterior edges of the occipital condyles (Figure 8).

Table 6. The angles measured in this study and the landmarks used.

Angles	Landmarks	Code
Flower Angle	(basion-prosthion)^(basion-nasion)	Flower_Angle
Middle Muzzle Angle	(basion-rhinion)^(basion-nasion)	ba_rhi_ba_n
Orbital plane^Frankfurt's plane	(inferior margin of each orbit- superior margin of the left orbit)^(porion-porion-inferior margin of the left orbit)	Frank_orbital_plane
Occipital plane^Frankfurt's plane	(inion- posterior occipital condyles)^(porion-porion- inferior margin of the left orbit)	Frank_o_i

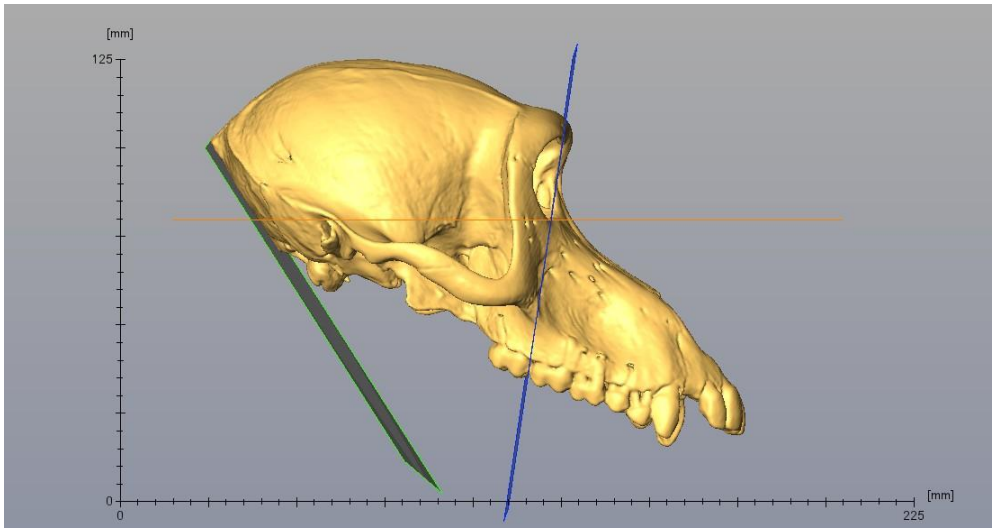

Figure 8. The three planes used to measure the Orbital plane(blue) ^Frankfurt's plane (orange) angle and Occipital plane(green)^Frankfurt's plane angle. Skull of *P. hamadryas* PRICT-424 KUPRI processed in Avizo software.

Based on the differences of the maxillary and lacrimal fossae between *Papio* and *Macaca* some observations were also made. For each specimen the maxillary fossa was characterized as deep or shallow and the position of the lacrimal fossa was characterized as being only inside the lacrimal bone or in contact with the frontal processor of the maxilla. The formation of the nuchal lines and the anterior temporal lines were also observed. The nuchal line can be strong or weak; it can turn upwards across the midline which leads the occipital view of the cranium to look upturned or can turn downwards giving a teardrop shape (Gilbert, 2007). The anterior temporal lines are characterized as convergent or divergent at the anterior portion of the cranium and oblique or parallel if they continue down the posterior portion.

In the specimens of the extant taxa, as well as in the fossil cranium it was possible to make almost all the above mentioned measurements. However, the fossil cranium DFN3-150 is moderately deformed and mediolaterally compressed. Compared to the left side, the right one is slightly sifted leading to an overlap of the palatal bone. In general, the palatal breadth was measured in three placements of the palatal area (Bicanine breadth, Bimolar breadth and Middle M^3 breadth as described in Table 4). To calculate the overall palatal breadth, the overlap was measured and then added to the palatal breadth. On each of the three placements of the palatal area a plane, parallel to the placements and almost vertical to the palate, was set using the Avizo tool ‘’Ortho Slice’’. Afterwards the scanning images in front of the selected planes were removed and the image of the inner structure of the cranium parallel to each plane was revealed (Figure 9) allowing us to measure the overlap of the palatal bone. Hence the ‘overlap distance’ was added to the palatal breadth for each placement.

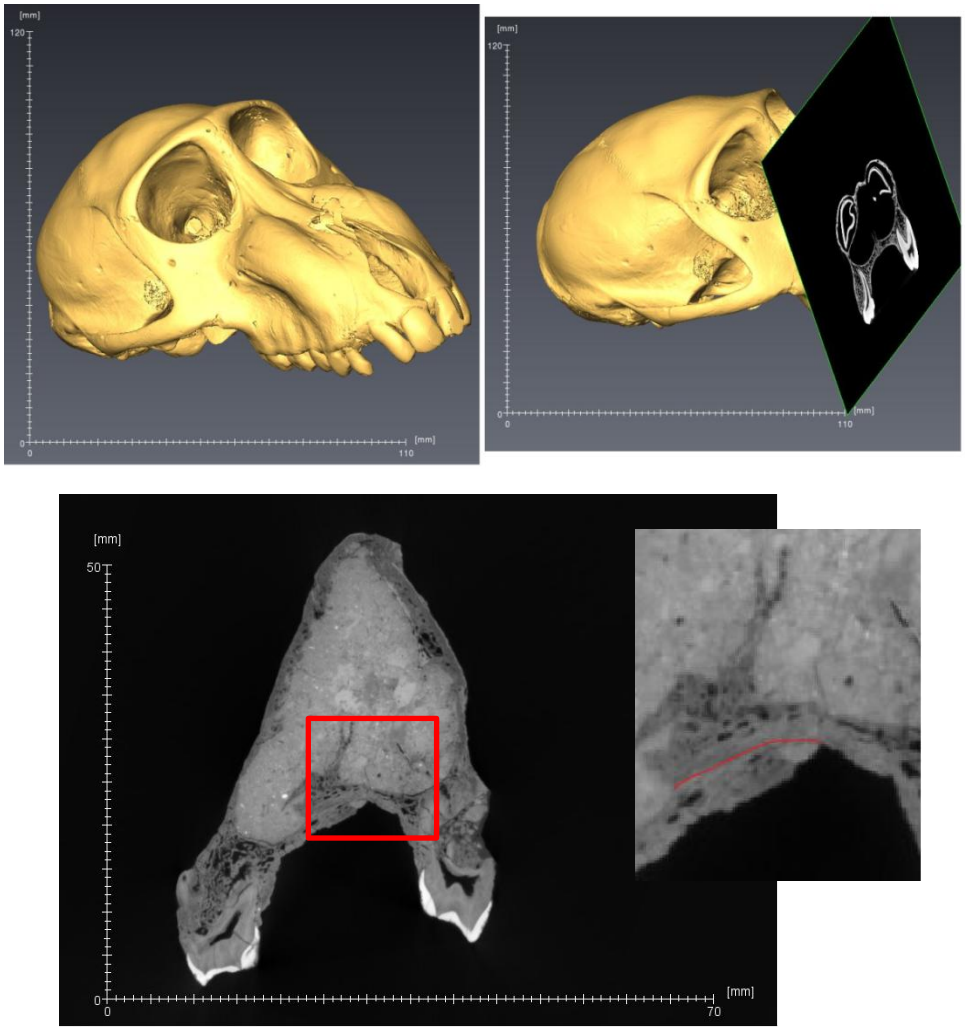

Figure 9. MicroCT images of *P. anubis* C2; using Avizo software a plane on the level of M^1 was created, the scanning images in front of the selected planes were removed and the inner morphology of the cranium is revealed (top). The same technic was used for the fossil DFN3-150 (bottom), where the palatal overlap of the fossil can be seen at the level of M^1.

Inner Measurements

In order to study the inner morphology of the craniums only the 3D images were used. At this phase the study focused on the maxillary sinuses that are formed in the maxillary bone, along the palatal area. Primarily it was investigated which of the specimens have maxillary sinuses and so each cranium was studied at the levels M^3, M^2 and M^1. Three planes parallel to these levels and almost vertical to the palate were created and the inner cranial morphology parallel to that planes was observed by ‘’Ortho Slice’’ module in Avizo.

None of the studied *Papio* specimens revealed features indicating a maxillary sinus as there are no empty cavities in the cancellous bone of the maxilla and no ostium. On the contrary, all of the studied specimens of *Macaca* have maxillary sinuses, restricted mainly to the molar region of the maxilla as pointed by Koppe *et al*. (1995). The fossil cranium of *Procynocephalus/Paradolichopithecus* DFN3-150 has also maxillary sinuses (Kostopoulos *et al*., *submitted*). Therefore, only the maxillary sinuses (MS) of the thirteen *Macaca* craniums and the fossil cranium from Dafnero 3 were studied.

The development of the maxillary sinuses was studied using the ‘’Image segmentation’’ module in Avizo and so the 3D images were able to be processed by two dimensional interactions in each slice. The in-slice interaction tools allowed the selection of voxels based on their gray scale threshold range, i.e. their density. The main feature that separates a maxillary sinus from the nasal cavity is the ostium (Mori *et al*., 2015) which isn’t easily identified, especially through the whole anteroposterior development of the sinuses. As a result, half of the nasal cavity alongside with one maxillary sinus was selected for each cranium (Figure 10).

In the extant Macaca species the maxillary sinuses are empty cavities and so it was easy to distinguish them from the bones. However, because the resolution of the scanning wasn’t the same for each cranium, in some specimens the maxillary sinuses’ images were more detailed than in others. Although the resolution of the 3D images of the fossil was very high, the empty cavities of the fossil are filled with sediment that provided a similar range in the gray scale as the fossilized bone. That made the selection of the maxillary sinus and half of the nasal cavity of the Dafnero 3 cranium a harder procedure (Figure 11).

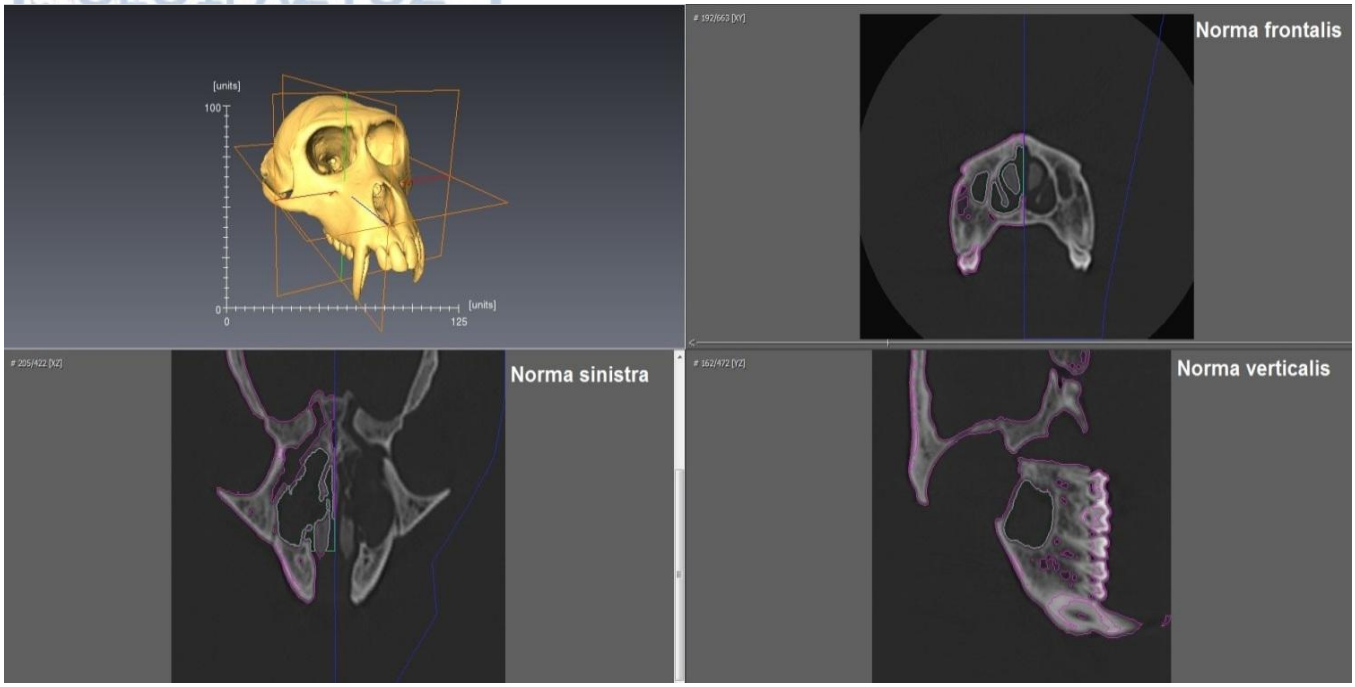

Figure 10.Segmenatation of *M. nemestrina* PRICT-1108 KUPRI with the Avizo software. The purple color indicates the selected bones while the green the selected maxillary sinus and half of the nasal cavity.

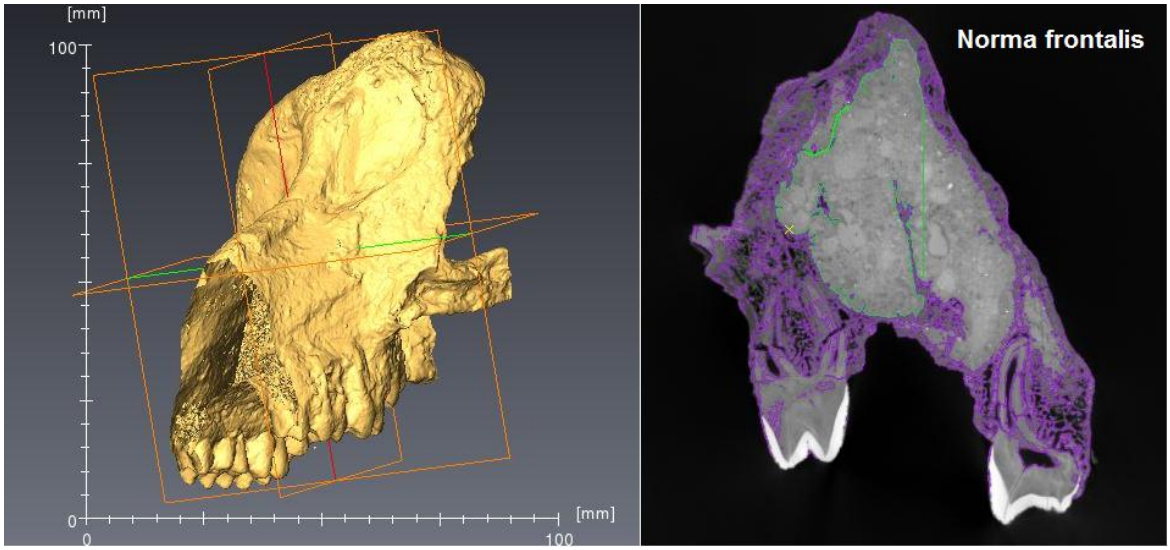

Figure 11. Segmentation of the viscerocranium of fossil DFN3-150 with Avizo software. The sediments and fossilized bones have similar range in gray scale. The selected fossilized bone is with purple color and with green the selected maxillary sinus and half of the nasal cavity.

The selected areas of half of the nasal cavity and the maxillary sinus were used to generate a surface with the ‘’Generate Surface’’ module in Avizo and they were saved as a Polygon File Forma ‘’.ply’’. They were later processed in Geomagic software as 3D normally flat polygons, which made it easier to distinguish the maxillary sinus from the nasal cavity. Using basic tools for each specimen, the sinus was selected and separated from the

nasal cavity, while the ‘’Fill hole’’ tool was used. Afterwards, the volume, the height and the length of the maxillary sinus were measured for each specimen (Figure 12).

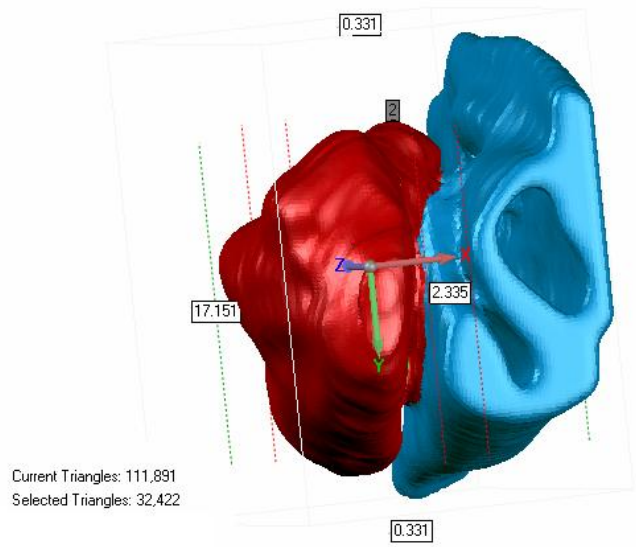

Figure 12. Half of the nasal cavity (blue) and the maxillary sinus (red) of the *Macaca nemestrina* PRICT-1108 KUPRI in Geomagic software. The maxillary sinus is selected and its height is measured.

Apart from the size of the maxillary sinuses a first approach on their shape among the extant *Macaca* species was also done in the current study. Their shape was observed based on the anteroposterior development alongside the nasal cavity. Because it was observed that maxillary sinuses have different dimensions, the total length of each sinus was divided by four and the first (anterior to posterior) two quarters were set as two placements. Using the Avizo software two planes vertical to the development of the sinuses were set in each of the two placements and with ‘’Ortho Slice’’. In these two placements the inner structure of the sinuses was observed. This procedure was done in only one specimen for each four studied *Macaca* species. The three-dimensional reconstruction of the MS and half of the nasal cavity, with transparent cranium, for these four specimens and the fossil DFN3-150 is shown at Figures I, II and III in the Appendix.

Statistics

To evaluate the biometric correlation of the fossil *Procynocephalus/Paradolichopithecus* DFN3-150 with either extant *Papio* or *Macaca*, all the 32 metrical data of the external measurements were statistically processed. Although the selected comparative species had approximately similar size with the fossil DFN3-150, normalization on all data was performed and so each variable was divided by the median of the measurement for all the specimens. The common logarithm of these data was used for the rest of the statistical analysis to minimize the statistical noise. A t-test was performed only with the data of the extant species. Using all the normalized data,

an UPGMA Hierarchical cluster analysis was performed with two methods, between-groups linkage cluster method with Pearson's correlation (BGL-PC) and Ward's method with Euclidean Distance coefficient (WM-ED), in the Statistical Package for the Social Sciences (SPSS) software. Also, a Principal Component Analysis (PCA) followed in PAleontological STatistics (PAST) software.

Regarding the inner measurements' data (volume/height/length of maxillary sinuses) from each specimen with maxillary sinuses, they were normalized by dividing each measurement with its geometric mean. A cluster analysis was conducted in SPSS and also a Boxplot in PAST.

CHAPTER 3. RESULTS

External measurements

The independent t-test was performed in order to compare the means between only the two extant genera on the same dependent variable (all the external measurements, including the angles). If a statistically high significant correlation between the two extant genera was revealed (>0.05), this measurement was excluded for further analysis as it could not help in reference to the fossil taxon. Table II in Appendix shows the results of the t-test and the remaining 29 normalized metrical measurements that were used in the following statistical analysis. Moreover, the results of the t-test show that differences in the muzzle and nasal area between the two extant genera are well described with the studied metrical distances. The distances of the frontomalare/temporale sutures as well as the orbital width seem to be also different among the two genera, whereas the orbital height is not. The position of the inion as described by the angle Occipital plane^Frankfurt's plane and the position of orbital plane as described by the angle Orbital plane^Frankfurt's plane aren't discriminating the two extant genera in contrast to the rest of the angles measured.

To identify biometric affiliation of the fossil DFN3-150 with the extant genera a UPGMA cluster analysis in SPSS was performed using only the remaining 29 normalized measurements. A between-groups linkage cluster method with Pearson's correlation (BGL-PC) in interval was used. Generally, between-groups linkage method uses the average distance of all data points within clusters as the distance between these clusters; Pearson's correlation attempts to draw a line of best fit through the data of two variables. Another cluster analysis was conducted using Ward's method with Euclidean Distance coefficient (WM-ED) as the measure of similarity. In Ward's method the distance is the distance of all clusters to the grand average of the sample and Euclidian Distance between two observations uses Pythagoras' formula for the right triangle. These two methods were used for all measurements to identify homogenous groups firstly among the extant species alone and later by introducing the fossil data into the analyses (Hammer and Harper, 2006). Dendrograms of the two methods were made in which the horizontal axis represents the distance or dissimilarity between the clusters and the vertical axis represents the specimens.

The dendrogram produced by cluster analysis with BGL-PC among only the extant taxa shows that all the *Papio* species are clustered together and separated from the macaques except of *M. sylvanus* PRICT-1152 KUPRI (Figure13). The juveniles *P. anubis* PRICT-733 KUPRI and *P. anubis* C2 are also outliers, fused rather arbitrarily at much higher distances in the *Papio* group, since they have relatively low values. The outlier for the *Macaca* group is *M. sylvanus* PRICT-1122 KUPRI. When the fossil measurements were introduced to the same cluster analysis (Figure 14), only the *M. sylvanus* PRICT-1152 KUPRI was an outlier in the *Papio* group and the *M. sylvanus* PRICT-1122 KUPRI in the *Macaca* group.

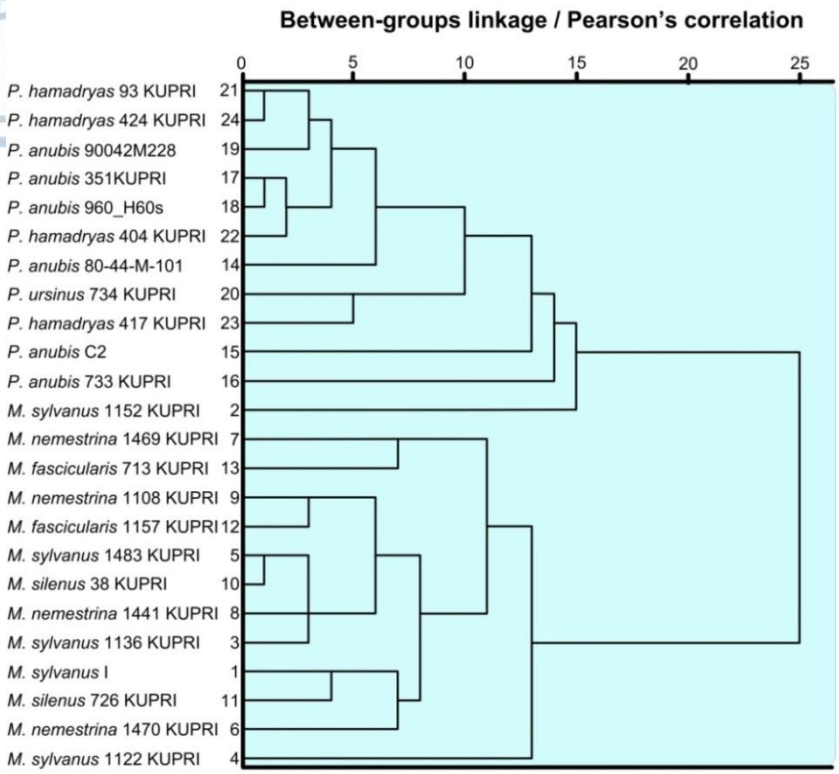

Figure 13. Dendrogram of hierarchical BGL-PC cluster analysis. Only the external cranial measurements of the extant genera were used.

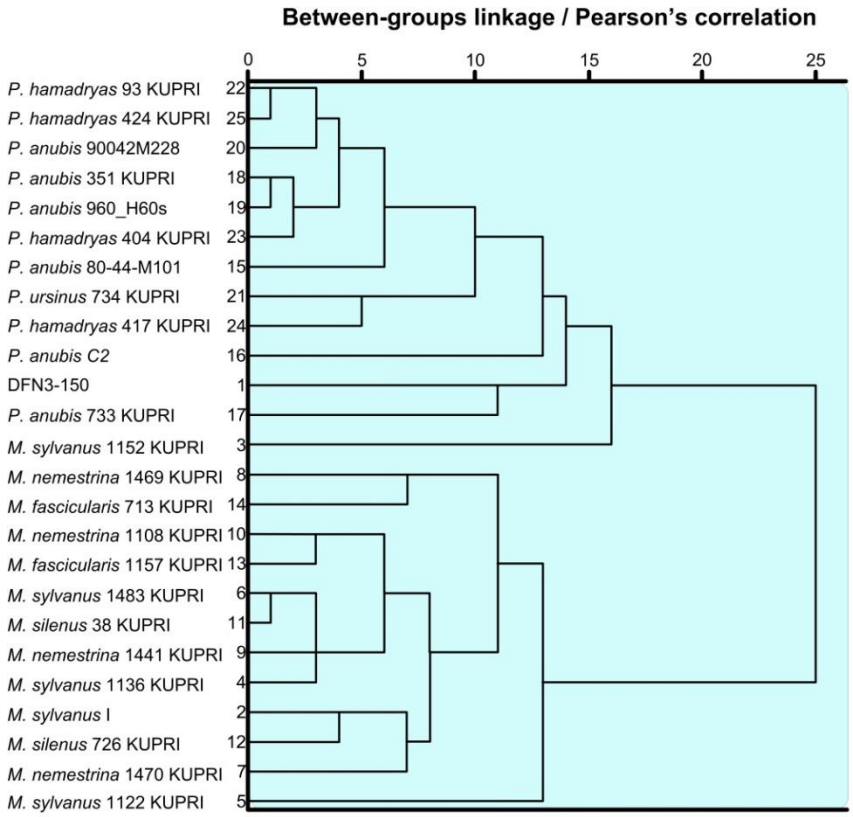

Figure 14. Dendrogram of hierarchical BGL-PC cluster analysis. The external measurements of the two extant genera and the fossil were used.

A BGL-PC cluster analysis was done using the variables (measurements) as clusters (R mode) to indicate the most important measurements used in the dendrograms of Figures 13 and 14. In Table 7 ‘’Coefficients’’ column shows that the representative variables (column ‘’Cluster 1’’ and ‘’Cluster 2’’) for the clustering are at the first four stages, because the decrease (since BLG-PC is for similarity measures) in the Coefficients between the fourth and the fifth stages is larger (Norušis, 2012). These Clusters are the measurements prosthion-nasion (Upper Facial height), nasion-nasospinale (Nasal height), porion-nasion (Nasion placement), porion-glabela (Glabela placement), inion-prosthion (Skull length), basion-prosthion (Facial length) and staphylion-prosthion (Palatal length). Based on these measurements, which seems to be focused on the main differences between the taxa i.e. the muzzle elongation (Strasser and Delson, 1987; Nishimura *et al*., 2007; Takai *et al*., 2008), the two male *M. sylvanus* (PRICT-1152 KUPRI and PRICT-1122 KUPRI) were found to be two specimens with higher values compared to all *Macaca* species, showing them as outliers in the *Papio* and *Macaca* group respectively.

Table 7. The complete linkage of the BGL-PC cluster. At the first stages of clustering the cases 7, 18, 13, 22, 2, 4 and 14 are used. These cases are respectively the measurements prosthion-nasion, nasion-nasospinale, porion-nasion, porion-glabela, inion-prosthion, basion-prosthion and staphylion-prosthion.

Stage	Cluster Combined		Coefficients	Stage Cluster First Appears		Next Stage
	Cluster 1	Cluster 2		Cluster 1	Cluster 2	
1	7	18	.995	0	0	6
2	13	22	.993	0	0	5
3	2	4	.992	0	0	4
4	**2**	**14**	**.987**	**3**	**0**	**7**
5	1	13	.967	0	2	10
6	7	19	.965	1	0	7
7	2	7	.955	4	6	13
8	12	16	.954	0	0	21
9	6	26	.954	0	0	19
10	1	3	.949	5	0	14
11	8	15	.947	0	0	17
12	5	11	.926	0	0	13
13	2	5	.914	7	12	14
14	1	2	.908	10	13	18
15	9	21	.902	0	0	22
16	28	29	.892	0	0	24
17	8	20	.891	11	0	23
18	1	17	.890	14	0	20
19	6	25	.877	9	0	27
20	1	24	.866	18	0	21
21	1	12	.852	20	8	23
22	9	23	.825	15	0	25
23	1	8	.819	21	17	25
24	10	28	.743	0	16	26
25	1	9	.734	23	22	27
26	10	27	.680	24	0	28
27	1	6	.663	25	19	28
28	1	10	.643	27	26	0

The dendrogram produced by cluster analysis with Ward's method (WM-ED) among only the extant taxa shows that all the *Papio* species are clustered together separately from the macaques (Figure 15). Even when the fossil's data are added to this cluster analysis, the two genera are obviously separated apart (Figure 16) and the fossil DFN3-150 is more closely related to the *Papio* specimens. In particular it is clustered with female *Papio* specimens, i.e. *P. hamadryas* PRICT-424 KUPRI, *P. anubis* 90042M228, *P. hamadryas* PRICT-93 KUPRI and *P. anubis* PRICT-733 KUPRI as well as two juvenile males, i.e. *P. anubis* C2 and *P.anubis* 80-44-M-101.

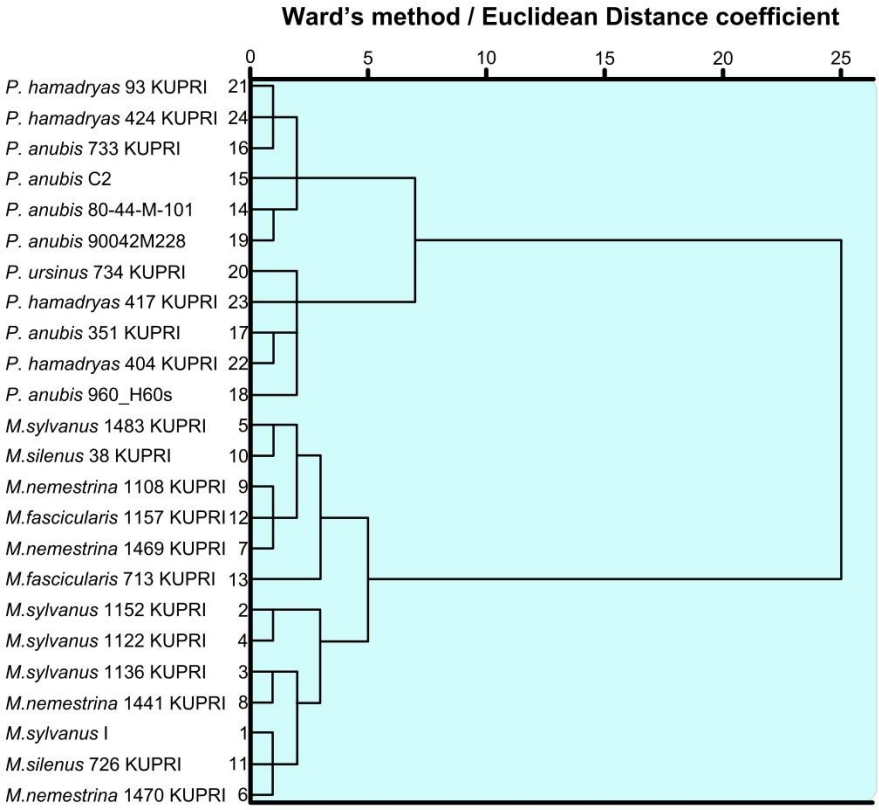

Figure 15. Dendrogram of hierarchical WM-ED cluster analysis between the external measurements of extant genera.

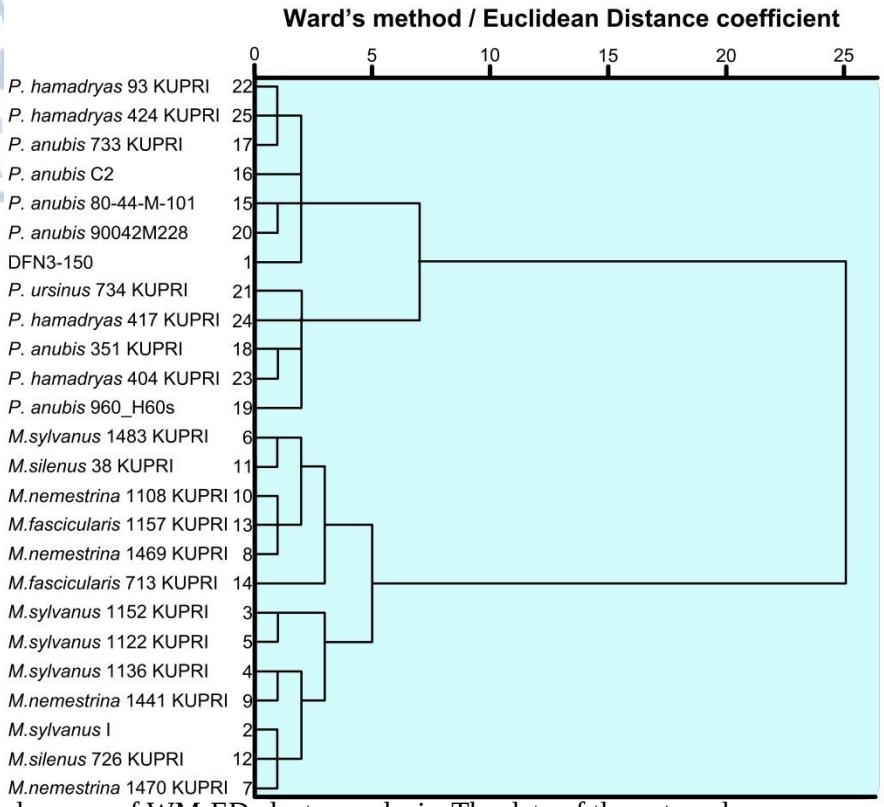

Figure 16. Dendrogram of WM-ED cluster analysis. The data of the external measurements from the two comparative genera and the fossil were used.

A WM-ED R mode cluster analysis was done to evaluate the most important measurements used in Figures 15 and 16. After the first three stages of clustering the increase (since WM-ED is for distance measures) in the Coefficients column between two adjacent steps is larger (Norušis, 2012) and so the most important measurements for the clustering are porion-nasion (Nasion placement), porion-glabela (Glabela placement), inion-prosthion (Skull length), prosthion-nasion (Upper Facial height), basion-prosthion (Facial length) and basion-nasion (Basicranial length) (Table 8). Congruently with previous cluster analysis this method suggests again that the main differences are in the muzzle elongation (Strasser and Delson, 1987; Nishimura *et al*., 2007; Takai *et al*., 2008).

Table 8. The complete linkage of the WM-ED cluster. At the first stages of clustering the cases 13, 22, 2, 4 and 1 are used. These cases are respectively the measurements porion-nasion, porion-glabela, inion-prosthion, prosthion-nasion, basion-prosthion and basion-nasion.

Stage	Cluster Combined		Coefficients	Stage Cluster First Appears		Next Stage
	Cluster 1	Cluster 2		Cluster 1	Cluster 2	
1	13	22	.019	0	0	3
2	2	4	.051	0	0	7
3	**1**	**13**	**.099**	**0**	**1**	**5**
4	6	26	.153	0	0	9
5	1	3	.208	3	0	22
6	7	18	.269	0	0	20
7	2	14	.338	2	0	21
8	9	21	.410	0	0	14

9	6	25	.491	4	0	25
10	20	23	.576	0	0	14
11	8	15	.662	0	0	19
12	5	11	.750	0	0	17
13	16	17	.849	0	0	16
14	9	20	.965	8	10	22
15	27	28	1.086	0	0	18
16	12	16	1.216	0	13	19
17	5	24	1.355	12	0	21
18	10	27	1.509	0	15	24
19	8	12	1.675	11	16	23
20	7	19	1.841	6	0	28
21	2	5	2.023	7	17	23
22	1	9	2.237	5	14	25
23	2	8	2.474	21	19	27
24	10	29	2.713	18	0	26
25	1	6	2.960	22	9	26
26	1	10	3.322	25	24	27
27	1	2	3.842	26	23	28
28	1	7	4.738	27	20	0

Using both clustering methods, there were clearly two groups clustering the *Papio* and the *Macaca* specimens separately and grouping the DFN3-150 fossil with the *Papio*. Nonetheless, in all the dendrograms there was no interspecific clustering in either groups of Papionini.

Using the normalized 29 metrical measurements a Principal Component Analysis (PCA) was performed in PAleontological STatistics (PAST) software to evaluate and reduce the variables into principal components. The matrix of the data is considered homogenous, so the parametric method var-covar (variance-covariance) was preferred.

In this PCA the first principal component accounts for more than 84% of the variation in the data. The scatter plot is made using the first two principal components and the eigenvalues as scale. Estimating the data with a convex hull polygon, which is the smallest convex polygon where all the given points are enclosed (Hammer and Harper, 2006), shows a clear dispersion of the *Macaca* and *Papio* groups along the PC2 axis. DFN3-150 has an intermediate position between the two groups in the PCA space (Figure IV in Appendix). Plotting a 95% confidence ellipse, within which 95% of the data are expected to lie (Hammer and Harper, 2006), the two groups are set partly apart in the scatter plot (Figure 17). The *Macaca* specimens that are far away from the confidence ellipse's center of the *Macaca* group are the outliers *M. sylvanus* PRICT-1122 KUPRI and *M. sylvanus* PRICT-1152 KUPRI, the same outliers of the cluster analyses. Within the 95% confidence ellipse of the *Papio* group, and close to the center of it, lays the fossil DFN3-150.

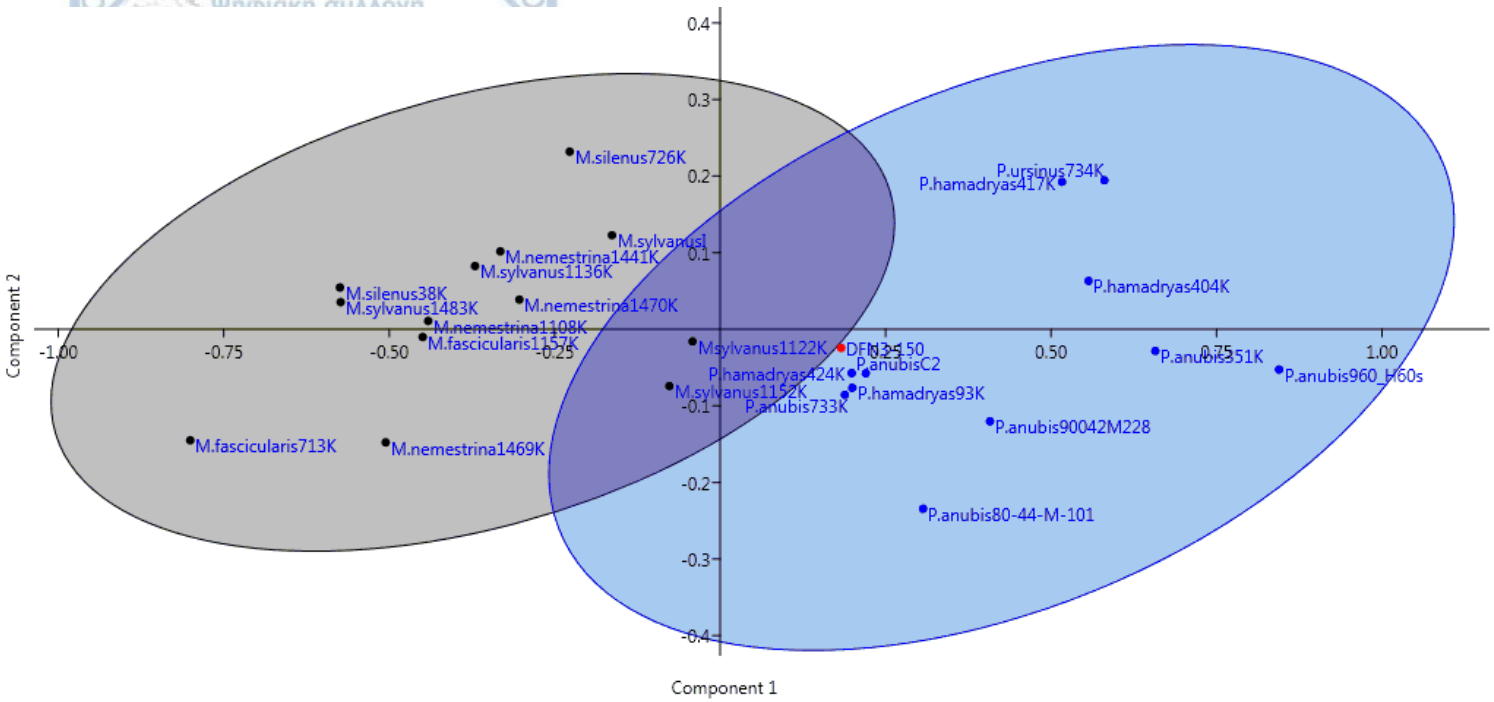

Figure 17. Scatter plot of the PCA using all the external measurements data and the 95% confidence ellipse that separates them in two groups. PC1 has 84,7% variance and PC2 5,4%.

Table III in Appendix presents the loadings of the first and second principal components showing how much each original variable contributes to each component. Based on that, PC1 is a hypothetical variable that increases sharply when the distances Nasal length (nasion-rhinion), Nasal height (nasion-nasospinale), Upper Facial height (prostion-nasion) increase and all the other distances increase as well.

The same procedure of the PCA was done with the data of the two extant genera alone. Although, the fossil was excluded the results were very similar with slightest differences in the loadings of the two first PC components.

Based on the present study DFN3-150 (Absolute measurements: Facial Length 118.54mm, Palatal Length 63.25mm, Nasal Length 45.25mm) has a more prominent than macaques muzzle (Absolute measurements: Facial Length range 76.31mm-102.16mm, Palatal Length range 40.37mm-59.62mm, Nasal Length range 19.33mm-36.57mm) but with no distinctive baboon-like maxillary fossa. Also in the studied *Papio* specimens (Absolute measurements: Facial Length range 108.86mm-159.24mm, Palatal Length range 66.78mm-102.06mm, Nasal Length range 44.53mm-81.14mm) the range for most of the muzzle's distances includes the values of DFN3-150. The neurocranium of DFN3-150 (Absolute measurements: Inion placement (o-i) 46.88mm, Cranial length 120.12mm) is longer than *Macaca* specimens (Absolute measurements: Inion placement range (o-i) 20.97mm-34.42mm, Cranial length 74.02mm-99.38mm) and within the range of *Papio* (Absolute measurements: Inion placement range (o-i) 34.86mm-57.36mm, Cranial length 98.16mm-125.25mm). In addition, according to Kostopoulos *et al*. (*submitted*) DFN3-150 cranium is referred to as a female subadult letting us to assume that most morphometric features should be further exaggerated with age and much further on male individuals.

Regarding few qualitative observations in the craniums, the lacrimal fossa is only in the lacrimal bone in all the studied *Papio* specimens and in DFN3-150 (Kostopoulos *et al*., *submitted* and pers. observations), while it is in the lacrimal bone and in contact to the frontal process of the maxilla in all macaques. The maxillary fossa is shallow in the *Macaca* specimens and DFN3-150, whereas deep in *Papio*, with a vast maxillary bulge in all the *Papio hamadryas* specimens. The formation of the nuchal lines and the anterior temporal lines don't state a clear distinction among the two living groups, making them ineffective in attributing the fossil specimen. Most of the *Macaca* show upturned and strong nuchal lines while in *Papio* there is no clear preference in the formation. Both in macaques and baboons the anterior temporal lines can be convergent or divergent, parallel or oblique even within the same species.

Inner measurements

Many authors use the presence of maxillary sinuses (MS) as an indication of affinity with *Macaca* species (Koppe and Ohkawa, 1999; Rae *et al*., 2002; Rae and Koppe, 2004; Rae, 2008). In the comparative studied specimens, only the *Macaca* species have MS; none of the studied *Papio* samples shows MS independently of age and/or sex (Figure 18). However, recent studies state that the presence of MS is also expected within Papionina (Nishimura *et al.*, 2014; Ito and Nishimura, 2016) and so this study was focused not only in the presence of MS, but their size and shape as well.

In order to identify homogenous groups of the maxillary sinus bearing species a cluster analysis was conducted. The first method used was BGL-PC cluster analysis with the normalized measurements (volume/height/length) only of the *Macaca* specimens' MS (Figure V in Appendix) and later the fossil DFN3-150 was added (Figure 19). In these dendrograms two groups appear: the first including specimens with relatively small maxillary sinus (*M. sylvanus* PRICT-1483 KUPRI, *M. silenus* PRICT-38 KUPRI, *M. fascicularis* PRICT-713 KUPRI) and *M. nemestrina* PRICT-1469 KUPRI, *M. silenus* PRICT-726 KUPRI and *M. nemestrina* PRICT-1441 KUPRI as outliers, and the second group uniting specimens with relatively larger sinuses (*M. sylvanus* I, *M. fascicularis* PRICT-1157 KUPRI, *M. sylvanus* PRICT-1152 KUPRI, *M. sylvanus* PRICT-1122 KUPRI, *M. sylvanus* PRICT-1136 KUPRI and *M. nemestina* PRICT-1470 KUPRI) with *M. nemestrina* PRICT-1108KUPRI as an outlier. When the fossil is included the two groups remain the same and DFN3-150 is clustered in the ''relatively smaller maxillary sinuses' size'' group.

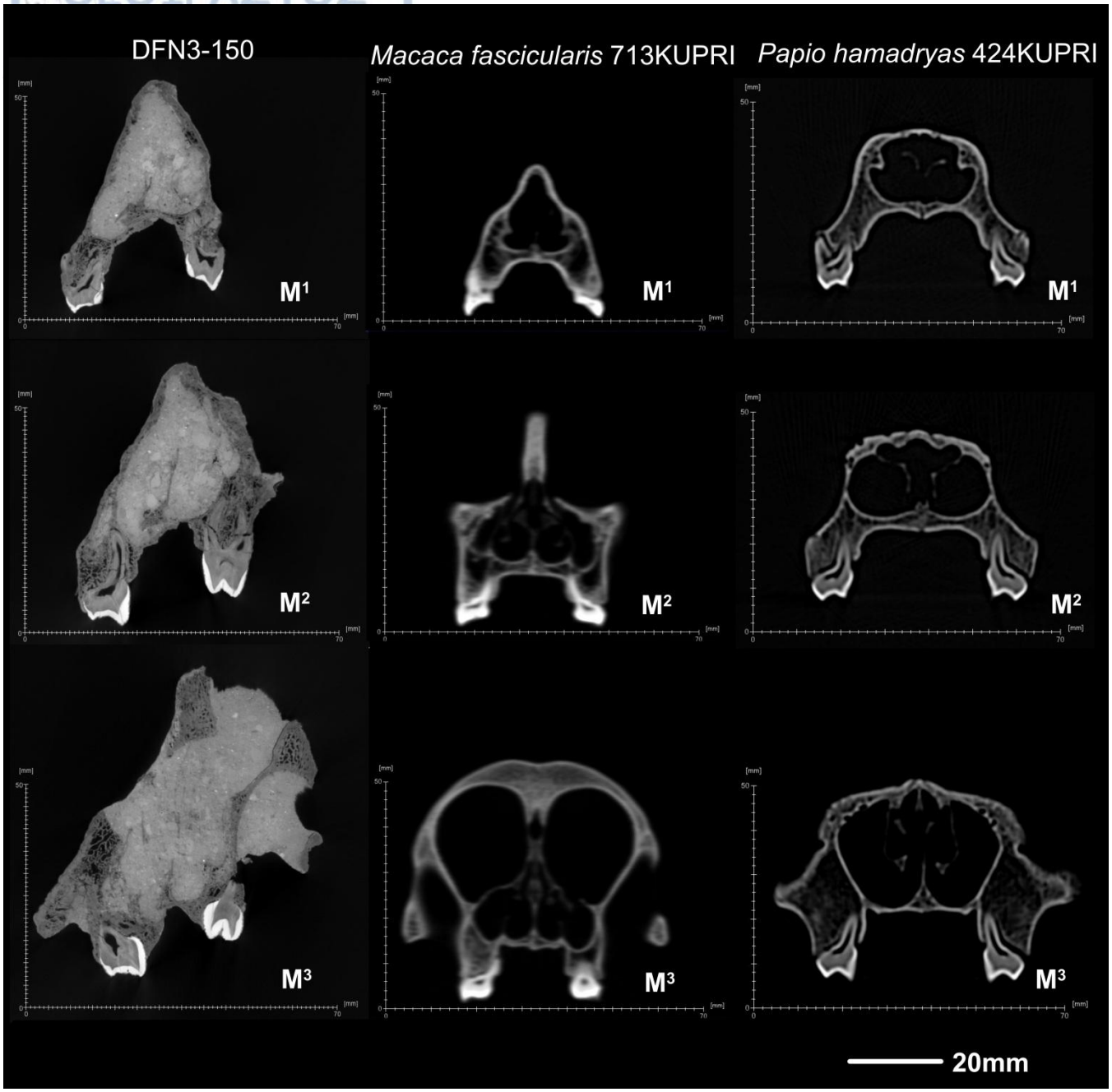

Figure 18: Coronal microCT images of DFN3-150 (left), *M. fascicularis* 713 KUPRI (middle) and *P. hamadryas* 424 KUPRI (right) at the level M^1, M^2 and M^3. The presence of maxillary sinus was investigated at these three levels for all the studied craniums. Images from Avizo software processed with Surfer software.

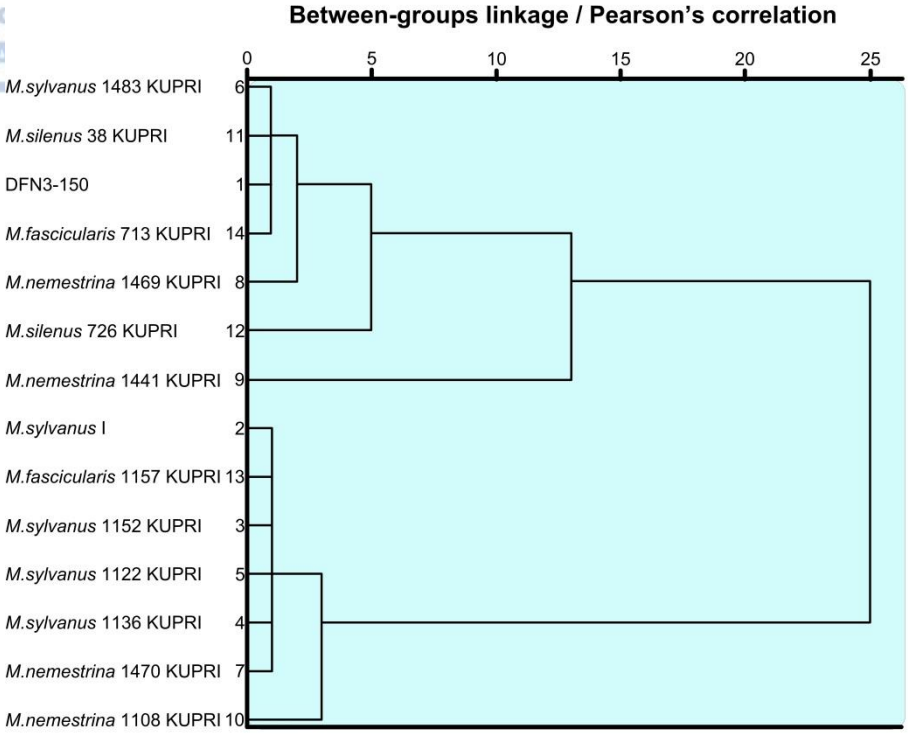

Figure 19. Dendrogram of BGL-PC cluster for the maxillary sinuses' dimensions of the *Macaca* species and DFN3-150 cranium.

The second method was WM-ED cluster analysis using only the maxillary sinuses' normalized measurements of the extant *Macaca* (Figure VI in Appendix) adding later the fossil data (Figure 18) provided again two main groups: one with small maxillary sinuses' size (*M. sylvanus* PRICT-1483 KUPRI, *M. silenus* PRICT-38 KUPRI, *M. nemestrina* PRICT-1469 KUPRI, *M. fascicularis* PRICT-713 KUPRI, *M. nemestrina* PRICT-1441 KUPRI and *M. silenus* PRICT-726 KUPRI) and another one of larger maxillary sinus size (*M. sylvanus* I, *M. fascicularis* PRICT-1157 KUPRI, *M. nemestrina* PRICT-1108KUPRI, *M. sylvanus* PRICT-1152 KUPRI, *M. sylvanus* PRICT-1136 KUPRI and *M. nemestina* PRICT-1470 KUPRI with *M. sylvanus* PRICT-1122 KUPRI as an outlier). When the fossil is added there is no change in these two groups and DFN3-150 is clustered in the ''relatively smaller size maxillary sinuses'' group.

Using both methods in clustering the size of the maxillary sinuses each species was not clustered in one group only, leading paraphyletic groups to emerge. Among the species of *Macaca* only *Macaca silenus* specimens are both in the ''relatively smaller maxillary sinuses'' group, while the rest species seem to have specimens with larger or smaller sinuses. The MS volume of *M. sylvanus* varied from 465.57mm^3 to 7997.26 mm^3, of *M. nemestrina* from 989.67mm^3 to 3918.51mm^3, of *M. silenus* from 455.65mm^3 to 875.28mm^3 and of *M. fascicularis* from 833.04mm^3 to 2644.16mm^3. The MS of the fossil cranium was small with 833.16 mm^3 volume, similar to the small sinuses of *M. silenus* and the minimum values of *M. sylvanus* and *M. fascicularis*

To visualize the wide distribution of the sinuses' size within each species, a boxplot using the normalized volume of the sinus (volume divided by its geometric mean) is given in Figure 21. *M. silenus* shows small sinus' volume and narrow distribution. *M. fascicularis* has a wider distribution and larger volume, while *M. nemestrina* and *M. sylvanus* show even larger values and ranges. *M. nemestrina* is being skewed with a tail towards larger volumes, while *M. sylvanus* towards smaller volumes, having also an outlier which is the male *M.sylvanus* PRICT-1122KUPRI. These results are in agreement with those of relative size of maxillary sinuses in macaques provided by Ito and Nishimura (2016). Nonetheless it is pointed out that the variations of size cannot be explained precisely and the whole nasal cavity size might provide more information. The fossil DFN3-150 shows small sinus' volume and is within the range of low values of all the studied *Macaca*.

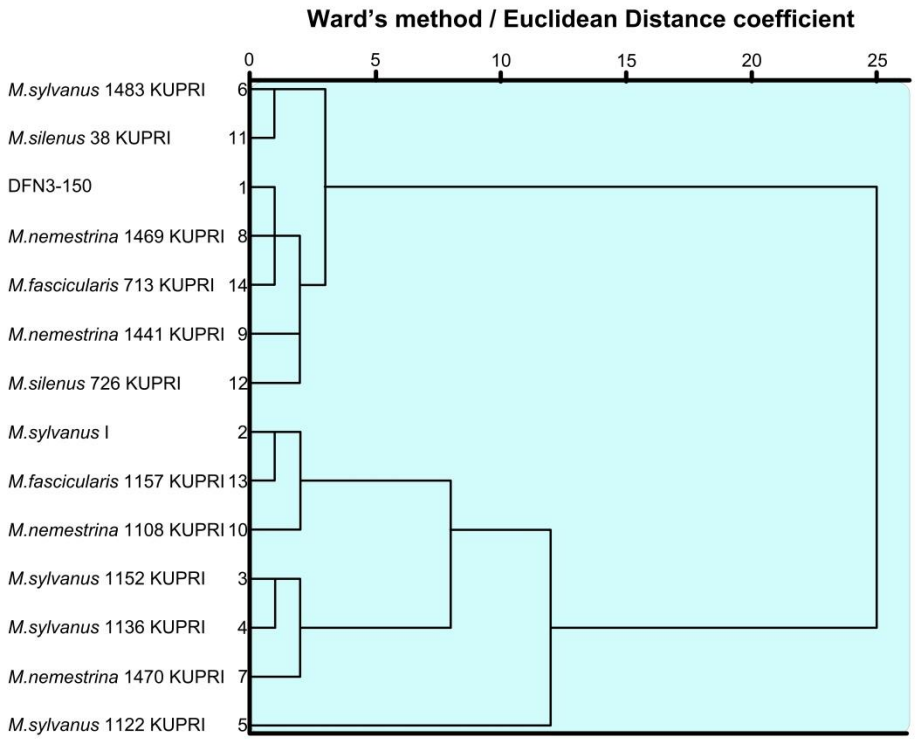

Figure 20. Dendrogram of WM-ED cluster using the maxillary sinuses' dimensions of the extant *Macaca* species and *Procynocephalus/Paradolichopithecus* DFN3-150.

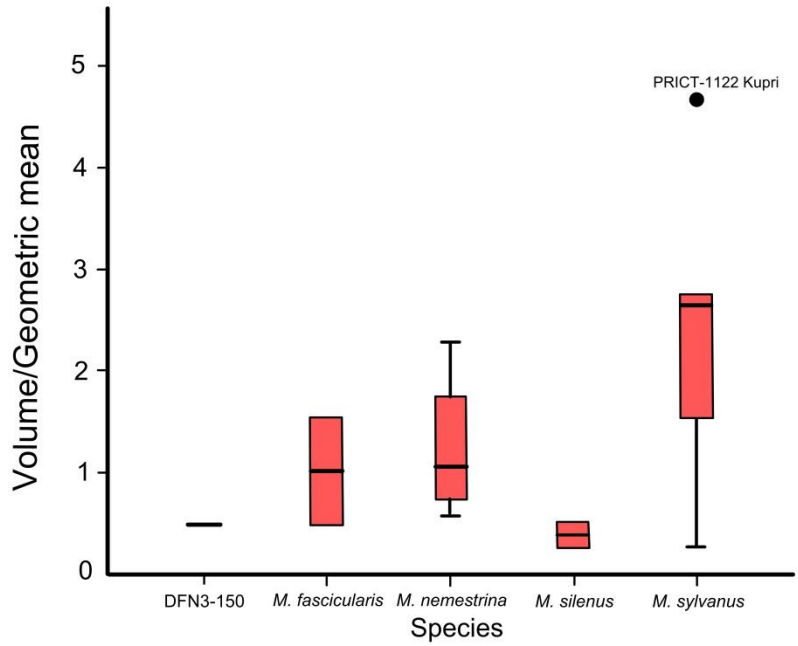

Figure 21. Boxplot of the maxillary sinuses' Volume divided by its Geometric mean in all the studied *Macaca* species and DFN3-150. The total range of the values, the maximal and minimal values (short horizontal lines) and the median (horizontal line inside each box) are plotted for each species (Hammer and Harper, 2006).

Since the maxillary sinuses' size showed such large interspecific dispersion, their shape was also investigated as a possible source of additional information. In particular the shape of the sinus vertical to its development at the first and second quarter of the total sinus' length is extracted (Figure 22). *M. sylvanus* appears to have a small nasal cavity compared to the MS which have a triangular shape that develops into a more quadrilateral shape. *M. nemesstrina* has similar development in the MS shape, yet the nasal cavity is larger. *M. silenus* also has a larger nasal cavity but the MS shape is teardrop-like in both the first and the second quarter studied. In the first quarter of the maxillary sinus' length in *M. fascicularis* the nasal cavity is smaller than the MS, which has again a teardrop-like shape. On the second quarter, however, the nasal cavity becomes even smaller and the MS is now triangularly shaped. Regarding the DFN3-150, it is relatively hard to estimate the shape since the cavities are filled with sediments. Approximately the nasal cavity of DFN3-150 is large along the whole length with teardrop-like MS in the first quarter that develops into a more quadrilateral/triangular shape. The study of the shape alongside the MS's length and of the relative size of the nasal cavity seems to be promising and further investigation is needed.

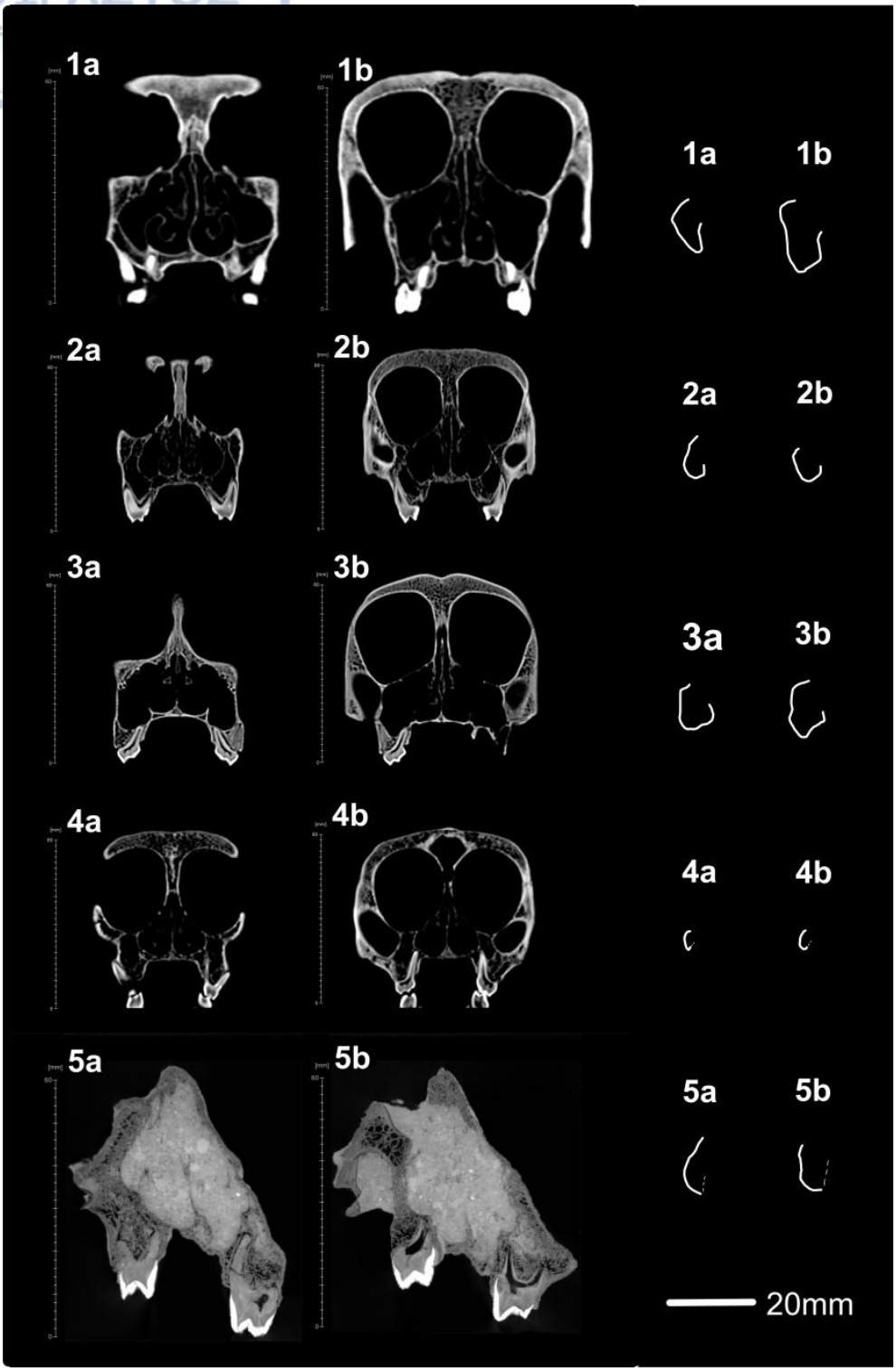

Figure 22. The shape of the maxillary sinus (MS) vertical to its development at the first (left) and second (right) quarter of the total sinus' length and the nasal cavity (NC) of the specimens *M. sylvanus* PRICT-1136 KUPRI (1a,1b), *M. fascicularis* PRICT-1157 KUPRI (2a,2b), *M. nemestrina* PRICT-1470 KUPRI (3a,3b), *M. silenus* PRICT-38 KUPRI (4a,4b) and DFN3-150 (5a,5b). Images by Avizo software on the left and on the right the shapes were created using Surfer software.

CHAPTER 4. DISCUSSION

Although the genera *Papio* and *Macaca* can be easily distinguished among living cercopithecines due to many outer and inner cranial differences (Singleton, 2002; Nishimura *et al*., 2007; Takai *et al*., 2008), the species *Procynocephalus/Paradolichopithecus* share many macaque and baboon like features. The well-studied European *P. arvenensis* has a moderately long muzzle and weekly developed maxillary fossae, which are macaque-like features, but shows also terrestrially adapted postcranial features resembling baboons (Szalay and Delson, 1979; Van der Geer and Sondaar, 2002; Jablonski, 2002; Nishimura *et al*., 2014). The fossil cranium DFN3-150 is generally considered quite similar to *Pr. wimani* (Kostopoulos *et al*., *submitted*) and has the lacrimal fossa engulfed only inside the lacrimal bone like *P. sushkini* (Trofimov, 1977), a character unclear in other fossils of the genus (Maschenko, 1994; Takai *et al*., 2008; Nishimura *et al*., 2014; Kostopoulos *et al*., *submitted*). Also, the fossil cranium of Dafnero has longer neurocranium compared to the face, similarly to *P. arvernensis, P. geticus*, *P.sushkini* (Kostopoulos *et al*., *submitted*) and the muzzle is moderately long as in *P. arvernensis* (Nishimura *et al*., 2014; Kostopoulos *et al*., *submitted*).

Based on the present study, the elongation of the muzzle and neurocranium (in absolute values) of DFN3-150 is within the range of *Papio* species and more prominent than macaques, with the lacrimal fossa being only in the lacrimal bone as in *Papio*. There is also a difference in the dentition since *Papio* have larger molars relative to premolars than *Macaca* (Fleagle and McGraw 1999, 2002; Gilbert, 2007), a feature shown in DFN3-150 and in many *Procynocephalus/Paradolichopithecus* specimens (Maschenko 1994; 2005; Takai *et al*., 2008). The fossil cranium DFN3-150 lacks the distinctive baboon-like maxillary fossa. The statistical analysis, after normalizing the data for the size differences among the taxa, clusters DFN3-150 closer to *Papio* species than *Macaca*. This classification is being mainly affected by the longer muzzle as well as the more elongated neurocranium (Figures 14 and 16). The PCA analysis scatter plot also places the fossil cranium DFN3-150 within the 95% confidence ellipse of the *Papio* group, and close to the center of it (Figure 17). Conclusively, the biometrical analysis identifies the fossil cranium DFN3-150 as having more biometric similarities with *Papio* specimens than macaques. It should also be noticed that DFN3-150 cranium belongs to a female subadult and therefore its morphometric features should be expected to be further exaggerated in adult males leading to a bigger resemblance to baboons.

The inner morphology of the cranium and the maxillary sinuses (MS) in particular were also investigated in order to reveal possible morphological phylogenetic relationships among the three taxa. The presence of the maxillary sinuses have been used to define phylogenetic correlation between extant and extinct taxa in primates (Andrews and Martin 1987; Gebo *et al*. 1997; Rossie *et al*. 2002; Nishimura *et al*. 2007; Rae, 2008; Takai *et al*. 2008; Nishimura *et al*. 2009; Pérez de los Ríos *et al*. 2012; Ito *et al*. 2014a; Nishimura *et al*. 2014). Along with the nasal cavity, the size/shape of MS have also been studied as possible aspects of adaptation in particular

climatic conditions (Shea, 1977;Rae and Koppe, 2003; Márquez and Laitman, 2008; Holton *et al*. 2011, 2013; Ito *et al*. 2015). Hypotheses suggest that maxillary sinuses are used in respiration, in thermoregulation or mastication (Blanton and Biggs, 1969; Witmer, 1997; Márquez, 2008; Rae and Koppe, 2008), but other studies failed to fully support these roles of the sinuses (Rae and Koppe, 2008; Butaric *et al*. 2010; Rae and Koppe, 2014; Curtis *et al*. 2015; Mori *et al*. 2015). MS is believed to have been lost in the common ancestor of the extant cercopithecoids and reoccurs only in macaque's lineage within the Cercopithecinae (Rae *et al*., 2002; Rae, 2008).

However, many studies suggested that the presence/absence of the MS as a phylogenetic and taxonomic character in primates is not reliable (Rae, 2008; Kuykendall and Rae, 2008). In Papionini, MS has been found in specimens of *Macaca* as well as of *Papio* and *Theropithecus* (Nishimura *et al*., 2014) showing that the presence of MS in a fossil specimen shouldn't point only to a *Macaca* affinity and that a thin maxillary body could instead indicate a correlation closer to Papionina. Also, Ito and Nishimura (2016) stated that the presence/absence of MS as a phylogenetic factor is still unclear and although maxillary sinuses may have no distinguished functions their loss or acquisition in taxa could be responsible for variability in changes of craniofacial components. In the genus of *Procynochephalus/Paradolichopithecus* only the craniums of *Paradolichopithecus sushkini* from Kuruksay, Tajikistan and *Procynocephalus*/*Paradolichopithecus aff. arvernensis* DFN3-150 from Dafnero, Greece have maxillary sinuses (Nishimura *et al*., 2010; Kostopoulos *et al*., *submitted*). In the current study only the specimens of *Macaca* and the fossil cranium DFN3-150 exhibits a MS but that shouldn't be an indisputable evidence of a closer affinity to macaques. Thus, the presence/absence of MS in the fossil cranium was not included as a phylogenetic factor.

Table 9. Presence of maxillary sinuses in the extinct genus of *Procynochephalus/Paradolichopithecus*.

Species of *Paradolichopithecus/Procynocephalus*	presence/absence of MS	Citation
P. arvernensis, Saneze, France	absent	Nishimura *et al*., 2009
P. sushkini, Kuruksay, Tajikistan	presence/large	Nishimura *et al*., 2007
P. gansuensis, Longdan, China	probably absent	Nishimura *et al*., 2010
P. geticus, Valea Graunceanului, Romania	-	-
Pr. winami, Xin'an, China	absent	Nishimura *et al*., 2014
Pr. subhimalayanus, India, Pakistan	-	-
DFN3-150, Dafnero, Greece	present/small	Kostopoulos *et al., submitted*; this study

The size of MS has been studied thoroughly and some suggest that smaller sinuses' volume depicts colder climatic conditions (Rae and Koppe, 2000), yet others that differences in MS volume show no clear climatic trend (Koertvelyessy, 1972; Rae and Koppe, 2003; Butaric *et al*., 2010; Rae *et al*., 2011; Butaric, 2015; Ito *et al*., 2015; Noback *et al*., 2016). Moreover, the MS continue to grow even after the individual reaches adulthood and thus MS's volume depends on the age of death (Ito *et al*., 2014a). The hypothesis that is gaining acceptance states that variation on the size of MS may depend on cumulative changes in craniofacial components (Ito and Nishimura,

2016) and so the surrounding architecture of the whole nasal cavity and maxilla needs to be studied to evaluate the phylogenetic and ecological implications of MS (Ito *et al*., 2014a; Ito and Nishimura, 2016). The MS volume should be considered as a combination of factors determined by the available space between the orbits and the dental arch (Zollikofer and Weissmann, 2008), or even changes in the facial structures (Lynnerup *et al*., 1999; Holton *et al*., 2013; Butaric and Maddux, 2015). It could also be the response of the whole area of the nasal cavity and maxilla to climatic pressures (Shea, 1977; Franciscus and Long, 1991; Roseman, 2004; Harvati and Weaver, 2006; Holton and Franciscus, 2008; Hubbe *et al*., 2009; Yokley, 2009; Noback *et al*., 2011; Evteev *et al*., 2016; Noback *et al*., 2016). Still not all specimens of *Procynochephalus/Paradolichopithecus* have MS even though they are found across the same range of latitude (Table 9). The present study questions not only the presence/absence of MS as a phylogenetic factor, as mentioned above, but the MS's size as well, since the size of MS appears to vary greatly even within the same species of the studied *Macaca* (Figure 21).

The shape of MS could vary because of the facial structure and the respiratory and masticatory components (Rae and Koppe, 2004), but could be irrelevant to the size and could therefore point out possible differences among genera. In the current study, the shape of the MS vertical to its development was examined in two different placements, which were decided based on each MS's length. The shape of MS and the size of the nasal cavity were observed and showed differences among species (Table 10). *M. sylvanus* and *M. fascicularis* with a wide range of MS's size appear to have small NC relative to MS, while *M. nemesstrina* which has same median in MS's size as *M. fascicularis* has a larger NC. *M. silenus* and DFN3-150 have small MS and larger nasal cavities (Figure 19 and Table 10). The triangular shape of MS seems to change into only quadrilateral (as seen in *M. sylvanus* and *M. nemesstrina*), whereas a tear-drop can change into either quadrilateral (DFN3-150), triangular (*M. fascicularis*) or even remain tear-drop (*M. silenus*) at the second quarter of the MS's length. This approach needs to be further tested for interspecific variations and also to be carried out in many more specimens thoroughly.

Table 10. Size of the nasal cavity (NC) relative to the maxillary sinus (MS) and the shape of MS in the first and second quarter of the total MS's length for four extant specimens of *Macaca* and the cranium fossil of DFN3-150.

Nasal cavity size / MS shape / Specimen (n=1)	first quarter of the MS's length	second quarter of MS's length
M. sylvanus PRICT-1136 Kupri	small NC / triangular MS	small NC / quadrilateral MS
M. fascicularis PRICT-1157 Kupri	small NC / tear-drop like MS	small NC / triangular MS
M. nemesstrina PRICT-1470 Kupri	large NC / triangular MS	large NC / quadrilateral MS
M. silenus PRICT-38 Kupri	large NC / tear-drop like MS	large NC / tear-drop like MS
Pr. aff. arvernensis DFN3-150	large NC / tear-drop like MS	large NC / quadrilateral MS

In order to test the phylogeny of DFN3-150 with *Macaca* and *Papio* we a posteriori extrapolated the studied characters to the three possible topographies determining their relationships. In the first hypothesis DFN3-

150 appears as the sister group of *Macaca* in agreement with Rae (2008), in the second of *Papio* and lastly in the third appears as a stem taxon of the *Macaca* - *Papio* lineage. The characters used to test all cladograms were based on the main morphological features of the subfamily Cercopithecinae which are significantly different in the extant genera (Delson, 2000; Singleton, 2002; Nishimura *et al*., 2007; Takai *et al*., 2008). According to Delson (2000) the derived conditions of Cercopithecinae are mainly focused in the cranium and dentition; the lacrimal fossa is in the lacrimal bone and the neurocranium is long, while the whole tribe of Papionini tends to have elongated face. A well distinguished difference in dentition is the elongation of the premolars relative to molars; this is seen in macaques, while *Papio* have larger molars to premolars (Fleagle and McGraw 1999, 2002; Gilbert, 2007).

As mentioned above the presence/absence of MS is not considered of phylogenetic value and so only these four morphological characters (position of lacrimal fossa, neurocranium and muzzle elongation and the ratio of molars' length to premolars) were used. The position of the lacrimal fossa enclosed only in the lacrimal bone corresponds to a primitive condition a(0) (Delson, 2000). A longer neurocranium relatively to the face -the distance from glabella to inion, parallel to the alveolar plane (Kostopoulos *et al*., *submitted*) is characteristic of all Cercopithecinae and so is considered as primitive state b(0) (Delson, 2000) and a more elongated muzzle -the distance from staphylion to prosthion- is an evolutionary tendency within the Papionini tribe and so is considered as advanced condition c(1) (Delson, 2000). Moreover, the elongated premolars are considered a primitive condition, d(0) that is shared among Macacina and *Mandrillus* and *Cercocebus*, while *Papio* have larger molars to premolars (Fleagle and McGraw 1999, 2002; Gilbert, 2007). Since only these four characters were used to test the affinities among the three genera, it is evident that the cladograms of Figure 23 represent just working hypotheses and in no case fully resolved phylogenetic trees.

The lacrimal fossa of the genus *Macaca* is in contact with the frontal process of the maxilla (Singleton, 2002; Nishimura *et al*., 2007; Takai *et al*., 2008), while the genus has a short neurocranium (Delson, 2000), and a shorter than *Papio* muzzle (Singleton, 2002; Nishimura *et al*., 2007; Takai *et al*., 2008), with elongated premolars to molars (Maschenko, 1994; Fleagle and McGraw 1999, 2002; Maschenko, 2005; Gilbert, 2007; Takai *et al*., 2008). On the contrary, *Papio* has the lacrimal fossa only in the lacrimal bone, a longer neurocranium, longer muzzle (Delson, 2000; Singleton, 2002; Nishimura *et al*., 2007; Takai *et al*., 2008) and longer molars to premolars (Maschenko, 1994; Fleagle and McGraw 1999, 2002; Maschenko, 2005; Gilbert, 2007; Takai *et al*., 2008). In DFN3-150, and in the cranium of *P. sushkini* (Tofimov, 1977; Maschenko, 1994), the lacrimal fossa is only in the lacrimal bone and the neurocranium's length is relatively shorter than the rest *Procynochephalus/ Paradolichopithecus* but still longer than the face (Kostopoulos *et al*., *submitted*). The molars are larger than premolars in DFN3-150 (Kostopoulos *et al*., *submitted*) as it is also seen in other specimens of *Procynocephalus/Paradolichopithecus* (Maschenko 1994; 2005; Takai *et al*., 2008) (Table 11).

The first group of cladograms (Figure 23) uses Wagner's optimality criteria (minimum constraints upon permitted character state changes) and the second uses the same characters of the taxa and the same evolutionary trends, but with Dollo's optimality criteria. Dollo's parsimony is different than Wagner's; all homoplasy must be accounted for as reversals to a more plesiomorphic state (Kitching *et al*., 1998) increasing the tree's length.

Table 11. The primitive states of the four characters used in the cladograms among the studied genera according to Delson (2000).

Genus \ Primitive state	lacrimal fossa only in lacrimal bone a(0)	relatively long neurocranium b(0)	relatively long muzzle c(0)	elongated premolars to molars d(0)
Macaca	advanced a(1)	advanced b(1)	primitive c(0)	primitive d(0)
Papio	primitive a(0)	primitive b(0)	advanced c(1)	advanced d(1)
DFN3-150	primitive a(0)	primitive b(0)	advanced c(1)	advanced d(1)

	a	b	c	d
Outgroup	0	0	0	0
Macaca	1	1	0	0
Papio	0	0	1	1
DFN3-150	0	0	1	1

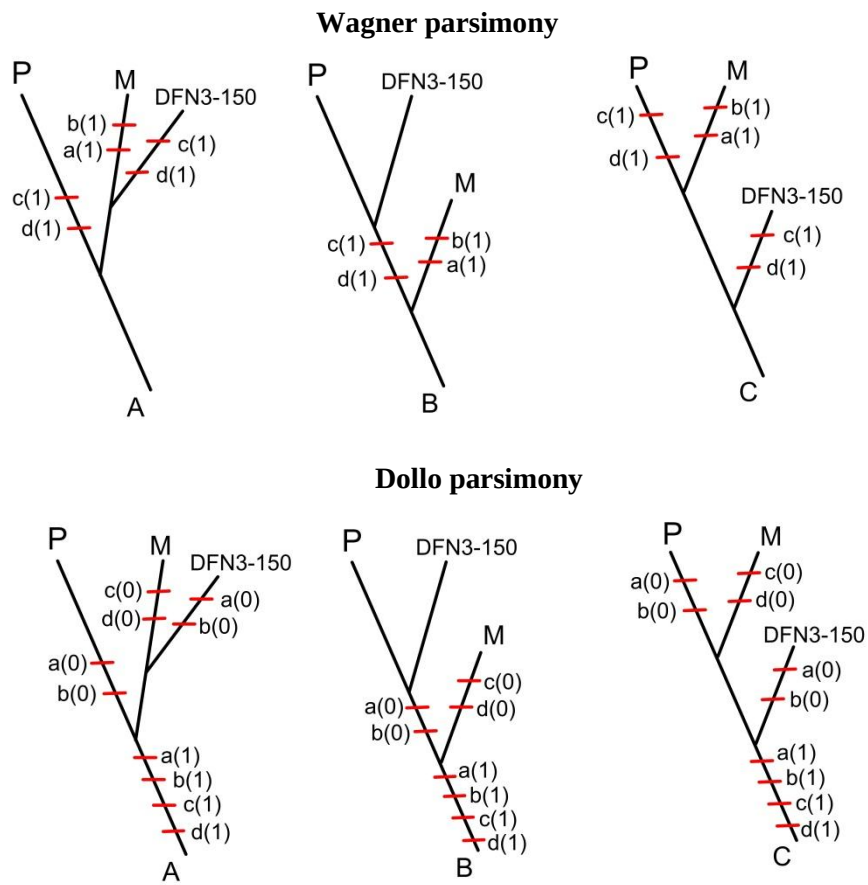

Figure 23. Three cladograms of the genera *Macaca* (M), *Papio* (P) and the *Procynochephalus/ Paradolichopithecus* (DFN3-150) based on the four characters (a,b,c,d) of the cranial features as described in Table 11 (lacrimal fossa, neurocranium's length, muzzle's elongation and premolars length relative to molars respectively) with Wagner's optimality criteria (above) and Dollo's criteriarion (below).

Based on this set of characters the most parsimonious scenario is the one indicating a closer relationship of DFN3-150 to *Papio* than *Macaca*. Apart from the postcranial features, that can be a result of similar locomotor adaption, *Procynochephalus/Paradolichopithecus* resembles *Papio* since the lacrimal fossa is enclosed only in the lacrimal bone and both have a primitive condition of an elongated neurocranium and a much longer muzzle than macaques. Also the molars are larger to premolars in many specimens of *Procynochephalus/Paradolichopithecus* (Maschenko 1994; 2005; Takai *et al*., 2008), another baboon like feature since macaques have primitive elongated premolars (Fleagle and McGraw 1999, 2002; Gilbert, 2007).

Supposing that a longer muzzle is an ecological adaption to similar environmental habitats in *Papio* and *Procynochephalus/Paradolichopithecus*, then the neurocranium's elongation could be considered as a mechanical response to the elongated muzzle. In Macacina the muzzle is primitively long, with primitively elongated premolars and the neurocranium has advanced to a shorter state; so if *Procynochephalus/Paradolichopithecus* is closely related to *Macaca* then it gained an advanced longer muzzle, more elongated molars to premolars and made an inversion having a longer neurocranium and another inversion for the lacrimal fossa as well.

The possibility that *Procynochephalus/Paradolichopithecus* is nested below the *Macaca – Papio* node could possibly explain the mixed characteristics of the genus. Yet, it seems to conflict with the FADs (first appearance data) of the involved taxa as *Macaca* appears much earlier (Late Miocene in North Africa; Delson, 1992) than *Papio* (2.2-1.8 Ma in South Africa; McKee, 1993; Gilbert *et al.*, 2014) or *Procynochephalus/ Paradolichopithecus* (3.2 Ma in central-western Europe; Rook *et al*., 2001; Elton and O'Regan, 2014; Gilbert *et al.*, 2014; Kostopoulos, *et al*., *submitted*).

During 2.5 Ma *Macaca* and *Procynochephalus/Paradolichopithecus* had already been in Europe and were following a northern dispersal route to inhabit eastern Eurasia (Takai *et al*., 2008). Meanwhile in Southern Africa, at Taung and Sterkfontein, the first species of *P. izodi*, *P. angusticeps* and *Parapapio broomi* appeared (McKee, 1993; Gilbert *et al.*, 2014). If *Procynochephalus/Paradolichopithecus* is a baboon-like macaque, then it would have diverged from European (Eurasian) macaques and followed a parallel evolution to *Papio* in Eurasia (Szalay and Delson, 1979; Maschenko, 1994; Jablonski, 2002; Ting *et al*., 2004; Frost *et al*., 2005; Takai *et al*., 2008; Nishimura *et al*., 2014; O'Shea *et al*., 2016; Kostopoulos *et al*., *submitted*). If *Procynochephalus/ Paradolichopithecus* is a macaque-like baboon then we have to admit an African origin before its appearance in Europe (>3.2Ma). Yet, no dispersal route from Africa during the 3-2 Ma for *Procynochephalus/ Paradolichopithecus* has ever been suggested and also the genus is believed to have originated in Europe (Necrasov *et al*., 1961; Jolly, 1967; Delson, 1974; Delson and Nicolaescu-Plopsor, 1975; Aguirre and Soto, 1978; Ardito and Mottura, 1987; Eronen and Rook, 2004). Nevertheless, geographic distribution of extant *Papio* exceeds Africa, with *P. hamadryas* being present in the Arabic peninsula (Rowe, 1996), whereas another member of Papionina (*Theropithecus*) did indeed invaded Eurasia later in the Pleistocene (Jablonski, 2002; Elton and O'Regan, 2014).

CHAPTER 5. CONCLUSIONS

The present study was done based on the cranium of a subadult female individual of *Procynocephalus*/*Paradolichopithecus* aff. *arvernensis*, that was found in Dafnero locality, North-West Greece. Delson (2000) characterized *Paradolichopithecus* as a baboon-like macaque derivative with similar facial morphology as macaques, but with larger more terrestrially adapted bodies, while Szalay and Delson (1979) stated that cranially *Paradolichopithecus* resembles macaques and postcranially baboons. As a result the genus *Procynochephalus/Paradolichopithecus* is considered to be a baboon-like macaque bearing morphological features of both genera; often its resemblance to *Papio* is thought to be due to ecological convergence (Szalay and Delson, 1979; Jablonski, 2002; Ting *et al*., 2004; Frost *et al*., 2005; Takai *et al*., 2008; Nishimura *et al*., 2014, O'Shea *et al*., 2016).

The external cranial morphology of the fossil cranium DFN3-150 was compared with the two extant genera of *Macaca* and *Papio*. Based on the statistical analysis and the biometrical data the fossil cranium from Dafnero-3 is more closely related to baboons. Moreover, the morphological features (position of lacrimal fossa, neurocranium and muzzle elongation and the ratio of molars' length to premolars) of the DFN3-150 are similar to most fossils of the genus *Procynochephalus*/*Paradolichopithecus*. Therefore it is suggested in this study that *Procynochephalus*/*Paradolichopithecus* could be a macaque-like ''baboon''. To support this new hypothesis further work needs to be done based on the evolvability of the craniofacial complex of the three genera. It is also proposed a further investigation and comparison with more craniums of the later Neogene Papionini and early extinct species of *P. izodi*, *P. angusticeps* and *Parapapio*. In particular, *Parapapio* and *P. izodi* are considered to have a steep anterorbital drop and well developed supraorbital torus compared to *Papio* (McKee, 1993); two features that should be thoroughly studied in the specimens of *Procynochephalus/Paradolichopithecus*.

The maxillary sinuses of the fossil and the extant macaques were also studied thanks to the 3D images produced after CT scanning and microCT scanning. Only the specimens of *Macaca* and the fossil cranium bear MS, but since they have been found in Papionini (Nishimura *et al*., 2014) the MS's presence/absence is considered of little phylogenetic value in the current study.

While studying the maxillary sinuses of the fossil cranium of DFN3-150 and correlating it to the extant *Macaca* species, the size of the MS has also been questioned. Each studied species of macaques has a wide range of MS size and so, overlaps in the size can't indicate one species (Figure 21). For this reason, the phylogenetic role of the MS's size is considered dubious.

A new approach to study the size of the nasal cavity in comparison with the MS and the shape of the MS has been proposed in order to further investigate the sinuses phylogenetic value. This method is relatively quick and easy and in the current study showed differences among the species. So, the shape of the MS alongside their length could be irrelevant to the size and probably point out differences among the species. This new method

needs to be further tested in many more specimens, while the understanding of the function of the MS and the factors leading to pneumatization of the face are also of highly importance.

ΠΕΡΙΛΗΨΗ

Το κρανιακό εύρημα DFN3-150, που βρέθηκε στην θέση Δαφνερό, κοντά στην Κοζάνη, αποτελεί ένα μεγαλόσωμο κερκοπίθηκο του Κατώτερου Πλειστοκαίνου που αποδίδεται στο είδος Procynocephalus aff. arvernensis. Εξωτερικά και εσωτερικά χαρακτηριστικά του κρανίου μετρήθηκαν και συγκρίθηκαν με 24 δείγματα αρτίγονων κερκοπιθήκων των γενών Papio και Macaca με σκοπό να συσχετισθούν φυλογενετικά τα τρία γένη. Με την βοήθεια εικόνων υψηλής ανάλυσης από αξονικούς τομογράφους πραγματοποιήθηκαν 32 μετρικές μετρήσεις της εξωτερικής δομής κάθε κρανίου. Η εσωτερική μορφολογία των κρανίων εστίασε στην ύπαρξη, το μέγεθος και το σχήμα των παραρρίνιων ιγμορείων. Τα παραρρίνια ιγμόρεια (MS) είναι εγκολπώσεις στην περιοχή γύρω από τη ρινική κοιλότητα και συνδέονται μαζί της μέσω μικρών ανοιγμάτων (ostium). Πιστεύεται πως τα παραρρίνια ιγμόρεια είναι ένα πρωτόγονο χαρακτηριστικό των κερκοπιθηκοειδών που εμφανίζεται ξανά στους Macaca. Σε όλες τις μετρήσεις έγινε απαλοιφή του μεγέθους των ειδών, καθώς κάθε τιμή διαιρέθηκε με τον διάμεσο όλων των δειγμάτων κάθε μέτρησης (εξωτερικές μετρήσεις) και τον γεωμετρικό μέσο κάθε μέτρησης (εσωτερικές μετρήσεις). Το δείγμα DFN3-150 φέρει εξωτερικά χαρακτηριστικά που μοιάζουν περισσότερο με τους μπαμπουίνους, αλλά έχει παραρρίνια ιγμόρεια, τα οποία είναι χαρακτηριστικά των μακάκων. Ωστόσο, πρόσφατες έρευνες έδειξαν ότι MS μπορεί να υπάρχουν και στα γένη Papio και Theropithecus οδηγώντας την παρούσα εργασία να μην θεωρεί σημαντικό φυλογενετικό κριτήριο την ύπαρξή τους στα δείγματα. Αμφίβολο είναι επίσης και το μέγεθος των MS ως φυλογενετικό χαρακτηριστικό καθώς το εύρος των μεγεθών εμφανίζεται πολύ μεγάλο για κάθε είδος που εξετάστηκε. Μια νέα μέθοδος, που προτείνεται στην παρούσα εργασία, και χρήζει περισσότερης διερεύνησης, είναι η αναλογία του μεγέθους της ρινικής κοιλότητας ως προς το μέγεθος των παραρρίνιων ιγμορείων και το σχήμα τους κατά μήκος της ανάπτυξης των τελευταίων. Η συσχέτιση των τριών γενών έγινε επιπλέον και με κλαδογράμματα σύμφωνα με τα κριτήρια φειδωλότητας των Wagner και Dollo, τα οποία έδειξαν να στηρίζουν την υπόθεση ότι το γένος Paradolichopithecus/Procynochephalus είναι εγγύτερο στους μπαμπουίνους από ότι στους μακάκες. Η νέα αυτή υπόθεση πρέπει να εξεταστεί ενδελεχώς και η μελέτη να εστιαστεί στην πορεία εξέλιξης των κρανιακών χαρακτήρων και στην μορφομετρική σύγκριση των κρανίων του γένους Paradolichopithecus/Procynochephalus με Νεογενή είδη των Papionina, όπως τα P. izodi, P. angusticeps και Parapapio.

ABSTRACT

Procynocephalus/*Paradolichopithecus* aff. *arvernensis*, DFN3-150, is a large cercopithecine monkey discovered from the Early Pleistocene of Dafnero, northwestern Greece. The external and internal cranial morphology was analyzed and compared to 24 specimens of modern Cercopithecinae from the genus of *Papio* and *Macaca* in order to evaluate the most closely related phylogenetic group. Using computed tomography CT and high-resolution micro-computed tomography microCT, 32 metrical measurements of the external features for each cranium were made. For the inner structure the presence, size and also shape of the maxillary sinuses were studied. Maxillary sinuses (MS) are paranasal sinuses that develop postnatally and invade the cancellous bone of the maxilla. It is hypothesized that the presence of maxillary sinus was lost in a common ancestor of the extant cercopithecoids and reoccurs in the lineage of *Macaca* in Cercopithecinae. All the data were standardized by dividing each measurements by its median (for the external) and the geometric mean (for inner) to exclude the shape differences correlated with size. DFN3-150 has a baboon-like appearance, more closely related with the *Papio* lineage as far as its external cranium features but it has maxillary sinuses which are typical for macaques. However, the presence of maxillary sinuses is not considered of high phylogenetic value since there are *Papio* and *Theropithecus* specimens that show pneumatization of the maxilla and in some cases maxillary sinuses. The size of MS showed a wide range in the *Macaca* specimens of the study, making it also a dubious characteristic. One new method of studying MS could be the size of the nasal cavity, relative to the MS, and the shape of the MS alongside their length, yet further investigation is needed. In addition, the affinities of the three studied genera were tested with cladograms using Wagner's and Dollo's optimality criteria, suggesting that *Procynochephalus/ Paradolichopithecus* is a macaca-like baboon. To support this new hypothesis further work needs to be done based on the evolvability of the craniofacial complex as well as morphometric comparisons with craniums of the later Neogene Papionini and early extinct species of *P. izodi*, *P. angusticeps* and *Parapapio*.

BIBLIOGRAPHY

Aguirre, E. and Soto, E., 1978. *Paradolichopithecus* in La Puebla de Valverde, Spain: Cercopithecoidea in European Neogene Stratigraphy. *Journal of Human* Evolution, 7, 559-565.

Alba, D., Colombero, S., Delfino, M., Martínez-Navarro, B., Pavia, M. and Rook, L., 2014. A thorny question: The taxonomic identity of the Pirro Nord cervical vertebrae revisited. *Journal of Human Evolution*, 76, 92-106.

Andrews, P. J. and Martin, L., 1987. Cladistic relationship of extant and fossil hominoids. *Journal of Human Evolution*, 16, 101-118.

Ardito, G. and Mottura, A., 1987. An overview of the geographic and chronologic distribution of West European cercopithecoids. *Human Evolution*, 2, 29-45.

Blanton, P. and Biggs, N., 1969. Eighteen hundred years of controversy: the paranasal sinuses. *American Journal of Anatomy*, 124, 135-148.

Bolomey, A., 1965. Die Fauna zweier villafrankischer Fundstellen in Rumanien. Vorläufige Mitteilungen Ber. *Berichte der geologischen Gesellschaft der DDR, Berlin*, 10, 77-88.

Butaric, L. N., 2015. Differential scaling patterns in maxillary sinus volume and nasal cavity breadth among modern humans. *The Anatomical Record*, 298, 1710-1721.

Butaric, L. N., and Maddux, S. D., 2015. Morphological covariation between maxillary sinus shape and the midfacial skeleton. In: *American Journal of Physical Anthropology* , 156, 96-97.

Butaric, L. N., McCarthy, R. C. and Broadfield, D. C., 2010. A preliminary 3D computed tomography study of the human maxillary sinus and nasal cavity. *American journal of physical anthropology*, 143, 426-436.

Cave, A. J. E., 1967. Observations on the platyrrhine nasal fossa. *American journal of physical anthropology*. 26, 277-288.

Curtis, A. A., Lai, G., Wei, F., and Valkenburgh, B., 2015. Repeated loss of frontal sinuses in arctoid carnivorans. *Journal of morphology*, 276, 22-32.

Dame, C. J. R., Chandra, A., Jones, A.S., Berend, N., Magnussen, J.S. and King, G.G., 2006. Airway dimensions measured from microcomputed tomography and high-resolution computed tomography. *European Respiratory Journal*, 28, 712-720.

De Vos, J., van der Made, J., Athanassiou, A., Lyras, G., Sondaar, P. Y. and Dermitzakis M. D., 2002. Preliminary note on the Late Pliocene fauna from Vatera (Lesvos, Greece). In: *Annales géologiques des Pays helléniques*, 39, No. 3, 37-70.

Delson, E., 1973. **Fossil colobine monkeys of the circum-Mediterranean region and the evolutionary history of the Cercopithecidae (Primates, Mammalia). Doctoral dissertation, Columbia University, New York, 856 pages.**

Delson, E., 1974. Preliminary review of cercopithecid distribution in the circum-Mediterranean region. *Mémoires du Bureau des Recherches Géologiques et Minières* (France), 78, 131-135.

Delson, E., 1992. Evolution of Old World monkeys. In: Martin R. D., Pilbeam D. and Jones J.S. (eds) *Encyclopedia of Human Evolution*. Cambridge University Press, Cambridge, 217-222.

Delson, E., 2000. Cercopithecinae. In: Delson, E., Tattersall, I., Van Couvering, J. A. and Brooks, A. S. (eds) *Encyclopedia of Human Evolution and Prehistory*, 2nd ed, New York, Garland, 166-171.

Delson, E. and Nicolaescu-Plopsor, D., 1975. *Paradolichopithecus*, a large terrestrial monkey (Cercopithecidae, Primates) from the Plio-Pleistocene of southern Europe and its importance for mammalian biochronology. *VIth Congress of Regional Committee of Mediterranean Neogene Stratigraphy, Bratislava*, 91-96.

Depéret, C., 1929. *Dolichopithecus arvernensis* Depéret: nouveau singe du Pliocène supérieur de Senèze (Haute-Loire). *Faculté des sciences*, Lyon 12, 5-12.

Elton, S. and O'Regan, H. J., 2014. Macaques at the margins: the biogeography and extinction of *Macaca sylvanus* in Europe. *Quaternary Science Reviews* 96, 117-130.

Eronen, J. T. and Rook, L., 2004. The Mio-Pliocene European primate fossil record: dynamics and habitat tracking. *Journal of Human Evolution*, 47, 323-341.

Evteev, A., Cardini, A. L., Morozova, I. and O'Higgins, P., 2014. Extreme climate, rather than population history, explains mid-facial morphology of northern Asians. *American journal of physical anthropology*, 153, 490-462.

Fleagle, J.G. and McGraw, W.S., 1999. Skeletal and dental morphology supports diphyletic origin of baboons and mandrills. *Proceedings of the National Academy of Sciences*, 96, 1157-1161.

Fleagle, J.G. and McGraw, W.S., 2002. Skeletal and dental morphology of African papionins: unmasking a cryptic clade. *Journal of Human Evolution*, 42, 267-292.

Fountoulis, I., Markopoulou-Diakantoni, A., Mpakopoulou, A., Moraiti, E., Mikrou, M. P. and Saroglou, X., 2001. The presence of marine Pliocene sediments in the Messohelenic trough (Pramoritsa banks, Grevena, Greece). *Bulletin of the Geological Society of Greece*, 24, 603-612.

Franciscus, R. G. and Long, J. C., 1991. Variation in human nasal height and breath. *American Journal of Physical Anthropology*, 85, 419-427.

Frost, S. R., Ting, N., Harcourt-Smith, W. and Delson, E., 2005. Positional and locomotor behavior of *Paradolichopithecus arvernensis* as inferred from the functional morphology of the postcrania (abstract). *American Journal of Primatology*, 66, 134-135.

Gebo, D. L., MacLatchy, L., Kityo, R., Deino, A., Kingston, J. and Pilbeam, D. R., 1997. A hominoid genus from the early Miocene of Uganda. *Science*, 276, 401-404.

van der Geer, A. A. E. and Sondaar, P. Y., 2002. The postcranial elements of 653 *Paradolichopithecus arvernensis* (Primates, Cercopithecidae, Papionini) from Lesvos, Greece. In: *Proceedings of the International Workshop, On Late Plio/Pleistocene extinctions and evolution in the Palearctic. The Vatera site, Vatera, Lesvos. Annales Géologiques des Pays Helleniques*, 39, 39, 71-86.

Gilbert, C. C., 2007. Craniomandibular morphology supporting the diphyletic origin of mangabeys and a new genus of the Cercocebus/Mandrillus clade, Procercocebus. *Journal of Human Evolution*, 53, 69-102.

Gilbert, C. C., 2013. Cladistic analysis of extant and fossil African papionins using craniodental data. *Journal of Human Evolution*, 64, 399-433.

Gilbert, C. C., Bibi, F., Hill, A. and Beech, M.J., 2014. Early guenon from the late Miocene Baynunah Formation, Abu Dhabi, with implications for cercopithecoid biogeography and evolution. *Proceedings of the National Academy of Sciences*, 111, 10119-10124.

Groves, C., 2000. The phylogeny of the cercopithecoidea. In: Whitehead, P. F. and Jolly, C.J. (eds.) *Old World Monkeys*. Cambridge University Press, Cambridge, 77-98.

Groves, C., 2001. *Primate Taxonomy*. Smithsonian Institution Press, Washington, DC, USA, 350 pages.

Hammer, Ø. and Harper, D. A. T., 2006. *Paleontological Data Analysis*. Blackwell Publishing, Malden, Massachusetts, 351 pages.

Harris, E. E., 2000. Molecular systematics of the Old World monkey tribe Papionini: analysis of the total available genetic sequences. *Journal of Human Evolution*, 38, 235–256.

Harvati, K. and Weaver, T., 2006. Human cranial anatomy and the differential preservation of population history and climate signatures. *The Anatomical Record Part A: Discoveries in Molecular, Cellular, and Evolutionary Biology*, 288, 1225-1233.

Heintz, E., Delson, E. and Crusafont, M, 1971. Descubrimiento del género *Macaca* en el yacimiento de la Puebla de Valverde (Teruel). *Boletín de la Real Sociedad Española de Historia Natural. Sección Geológica*, 69, 299-302.

Heintz, E., Guérin, C., Martin, R. and Prat, F., 1974. Principaux gisements villafranchiens de France: listes fauniques et biostratigraphie. *Mémoires du Bureau de Recherches géologiques et minières*, 78, 169-182.

Holton, N. E. and Franciscus, R. G., 2008. The paradox of a wide nasal aperture in cold adapted Neandertals: a causal assessment. *Journal of Human Evolution*, 55, 942-951.

Holton, N., Yokley, T. R. and Butaric, L., 2013. The morphological interaction between the nasal cavity and maxillary sinuses in living humans. *The Anatomical Record*, 296, 414-426.

Holton, N. E., Yokley, T. R. and Franciscus, R.G., 2011. Climatic adaptation and Neandertal facial evolution: A comment on Rae et al. (2011). *Journal of Human Evolution*, 61, 624-627.

Hubbe, M., Hanihara, T. and Harvati, K., 2009. Climate signatures in the morphological differentiation of worldwide human populations. *The anatomical record*, 292, 1720-1733.

Ito, Ts., Kawamoto, Y., Hamada, Y., and Nishimura, T. D., 2015. Maxillary sinus variation in hybrid macaques: implications for the genetic basis of craniofacial pneumatization. *Biological Journal of the Linnean Society*, 115, 333-347.

Ito, Ts. and Nishimura, T. D., 2016. Enigmatic diversity of the maxillary sinus in macaques and its possible role as a spatial compromise in craniofacial modifications. *Evolutionary Biology*, 43, 414-426.

Ito, Ts., Nishimura, T. D., Ebbestad, J. O. R., and Takai, M., 2014a. Computed tomography examination of the face of *Macaca anderssoni* (Early Pleistocene, Henan, northern China): implications for the biogeographic history of Asian macaques. *Journal of Human Evolution*, 72, 64-80.

Ito, Ts., Nishimura, T. D., Hamada, Y., and Takai, M., 2014b. Contribution of the maxillary sinus to the modularity and variability of nasal cavity shape in Japanese macaques. *Primates*, 56, 11-19.

Ito, Ts., Nishimura, T. D., Senut, B., Koppe, T., Treil, J., and Takai, M., 2009. Reappraisal of *Macaca* speciosa subfossilis from the Late Pleistocene of northern Vietnam based on the analysis of cranial anatomy. *International Journal of Primatology*, 30, 643-662.

Jablonski, N. G., 2002. Fossil Old World monkeys: the late Neogene radiation. In: Hartwig, W.C. (ed.) *The Primate Fossil Record*. Cambridge University Press, Cambridge, 255-299.

Jablonski, N. G. and Frost, S. R., 2010. Cercopithecoidea. In: Werdelin, L. and Sanders, W. J. (eds.), *Cenozoic mammals of Africa*. University of California Press, Berkeley, 393-428.

Jolly, C. J., 1967. The evolution of baboons. In: Vagtborg, H. (ed.) *The Baboon in Medical Research*, 2. University of Texas Press, Aistom, 23-50.

Kitching, I. J., Forey, P. L., Humphries, Ch. J, Williams, D. M., 1998. Cladistics. The theory and practice of parcimony analysis. Oxford University Press, 235 pages.

Koertvelyessy, T., 1972. Relationships between the frontal sinus and climatic conditions: a skeletal approach to cold adaptation. *American journal of physical anthropology*, 37, 161-172.

Kopp, G. H., Roos, C., Butynski, T. M., Wildman, D. E., Alagaili, A. N., Groeneveld, L. F. and Zinner, D., 2014. Out of Africa, but how and when? The case of hamadryas baboons (*Papio hamadryas*). *Journal of human evolution*, 76, 154-64.

Koppe, T. and Ohkawa, Y., 1999. Pneumatization of the facial skeleton in catarrhine primates. In: Koppe, T., Nagai, H. and Alt, K.W. (eds.) *The Paranasal Sinuses of Higher Primates: Development, Function, and Evolution*. Quintessence, Berlin, 77-119.

Koppe, T., Yamamoto, T., Tanaka, O., and Nagai, H., 1995. Investigations on the growth pattern of the maxillary sinus in Japanese human fetuses. *Okajimas folia anatomica Japonica*, 71, 311-318.

Kostopoulos, D.S., Kynigopoulou, Z., Guy, F., Koufos, G., Valentin, X., Merceron, G., *submitted*. A 2Ma-old baboon-like monkey from Northern Greece: Procynocephalus/*Paradolichopithecus* aff. arvernensis (Primates: Cercopithecidae). *submitted* in *Journal of Human Evolution*.

Koufos, G. D., 2001. The Villafranchian mammalian faunas and biochronology of Greece. *Bollettino- Societa Paleontologica Italiana*, 40, 217-223.

Koufos, G. D., Kostopoulos, D. S. and Koliadimou, K., 1991. Un nouveau gisement de mammiferes dans le Villafranchien de Macèdoine occidentale (Grèce). *Comptes Rendus de l'Academie des Sciences, Paris*, 313, 831-836.

Kuykendall, K. L., and Rae, T. C., 2008. Presence of the maxillary sinus in fossil Colobinae (Cercopithecoides williamsi) from South Africa. *The Anatomical Record*, 291, 1499-1505.

Lynnerup, N., Homøe, P. and Skovgaard, L.T., 1999. The frontal sinus in ancient and modern Greenlandic Inuit. *International Journal of Anthropology*, 14, 47-54.

Macchiarelli, R., Bondioli, L., Debenath, A., Mazurier, A., Tournepiche, J.F., Birch, W. and Dean, C., 2006. How Neaderthal molar teeth grew. *Nature*, 444, 748-751.

Maier, W., 2000. Ontogeny of the nasal capsule in cercopithecoids: a contribution to the comparative and evolutionary morphology of catarrhines. In: Whitehead, P.F. and Jolly, C.J. (eds.), *Old World Monkeys.* Cambridge University Press, Cambridge, 99-132.

Marigo, J., Susanna, I., Minwer-Barakat, R., Madurell-Malapeira, J., Moyà-Solà, S., Casanovas-Vilar, I., Robles, J. M. and Alba, D.M., 2014. The primate fossil record in the Iberian Peninsula. *Journal of Iberian Geology*, 40, 179-211.

Márquez, S., 2008. The paranasal sinuses: the last frontier in craniofacial biology. *The Anatomical Record*, 291, 1350-1361.

Márquez, S. and Laitman, J. T., 2008. Climatic effects on the nasal complex: a CT imaging, comparative anatomical, and morphometric investigation of *Macaca mulatta* and *Macaca fascicularis*. *Anatomical Record-Advances in Integrative Anatomy and Evolutionary Biology*, 291, 1420-1445.

Maschenko, E. N., 1994. Comparative morphological analysis of the skull and lower jaw of the late Pliocene baboon *Papio suschkini*. In: Tatarinov, L.P. (ed.) *Paleonteriologia*. Nauka, Moscow, 15-57 (in Russian).

Maschenko, E. N., 2005. Cenozoic primates of eastern Eurasia (Russia and adjacent areas). *Anthropological Science*, 113, 103-115.

McKee, J.K., 1993. Taxonomic and evolutionary affinities of Papio izodi fossils from Taung and Sterkfontein. *Palaeont. Afr*, 30, 43-49.

von Meyer, H., 1848. In: Bronn, H.G. (ed.), Index Palaeontologicus, Stuttgard: E.Schweizerbart.

Mori, F., Hanida, S., Kumahata, K., Miyabe-Nishiwaki, T., Suzuki, J., Matsuzawa, T., and Nishimura, T. D., 2015. Minor contributions of the maxillary sinus to the air-conditioning performance in macaque monkeys. *Journal of Experimental Biology*, 218, 2394-2401.

Necrasov, O., Samson, P. and Rădulesco, C., 1961. Sur un nouveau singe catarrhinien fossile, découvert dans un nid fossilifère d'Olténie (R.P.R.). *Analele Stiintifice Universitatii "Al. I. Cuza" Iasi, Sect. II*, 7, 401-416.

Nishimura, T. D. and Ito, Ts., 2014. Aplasia of the maxillary sinus in a Tibetan macaque (Macaca thibetana) with implications for its evolutionary loss and reacquisition. *Primates*, 55, 501-508.

Nishimura, T. D., Ito, Ts., Yano, W., Ebbestad, J. O. R. and Takai, M. 2014. Nasal architecture in *Procynocephalus wimani* (Early Pleistocene, China) and implications for its phyletic relationship with *Paradolichopithecus*. *Anthropological Science* 122, 101-113.

Nishimura, T. D., Senut, B., Prieur, A., Treil, J. and Takai, M., 2009. Nasal architecture of *Paradolichopithecus arvernensis* (late Pliocene, Senèze, France) and its phyletic implications. *Journal of Human Evolution*, 56, 213-217.

Nishimura, T. D., Takai, M. and Maschenko, E., 2007. The maxillary sinus *of Paradolichopithecus sushkini* (late Pliocene, southern Tajikistan) and its phyletic implications. *Journal of Human Evolution*, 52, 637-646.

Nishimura, T. D., Takai, M., Tsubamoto, T., Egi, N. and Shigehara, N., 2005. Variation in maxillary sinus anatomy among platyrrhine monkeys. *Journal of Human Evolution*, 49, 370-389.

Nishimura, T. D., Zhang, Y. and Takai, M., 2010. Nasal Anatomy of *Paradolichopithecus gansuensis* (Early Pleistocene, Longdan, China) with comments on phyletic relationships among the species of this genus. *Folia primatologica*, 81, 53-62.

Noback, M. L., Harvati, K. and Spoor, F., 2011. Climate related variation of the human nasal cavity. *American journal of physical anthropology*, 145, 599-614.

Noback, M. L., Samo, E., van Leeuwen, C. H., Lynnerup, N., and Harvati, K., 2016. Paranasal sinuses: A problematic proxy for climate adaptation in Neanderthals. *Journal of Human Evolution*, 30, 1-4.

Norušis, M. J., 2012. *IBM SPSS statistics 19 statistical procedures companion*. Prentice Hall, 672 pages.

O'Sea, N., Delson, E., Pugh, K. D. and Gilbert, C. C., 2016. Phylogenetic analysis of *Paradolichopithecus*: Fossil baboon or macaque? *The 85th Annual Meeting of the American Association of Physical Anthropologists 2016* (abstract).

Pérez de los Ríos, M., Moyà-Solà, S., and Alba, D. M., 2012. The nasal and paranasal architecture of the Middle Miocene ape *Pierolapithecus catalaunicus* (Primates: Hominidae): Phylogenetic implications. *Journal of Human Evolution*, 63, 497-506.

Qiu, Z., Deng, T. and Wang, B., 2004. Early Pleistocene mammalian fauna from Longdan, Dongxiang, Gansu, China. *Palaeontologia Sinica 27 (191 New Series C)*, 1-198. *Plate*, 1–34 (in Chinese with English summary).

Raaum, R. L., Sterner, K. N., Noviello, C. M., Stewart, C. B. and Disotell, T. R., 2005. Catarrhine primate divergence dates estimated from complete mitochondrial genomes: concordance with fossil and nuclear DNA evidence. *Journal of Human Evolution*, 48, 237-257.

Rae, T. C., 2008. Paranasal pneumatization in extant and fossil Cercopithecoidea. *Journal of Human Evolution*, 54, 279-286.

Rae, T. C. and Koppe, T., 2000. Isometric scaling of maxillary sinus volume in hominoids. *Journal of Human Evolution*, 38, 411-423.

Rae, T. C. and Koppe, T., 2003. The term ‘‘lateral recess’’ and craniofacial pneumatization in Old World monkeys (Mammalia, Primates, Cercopithecoidea). *Journal of Morphology*, 258, 193-199.

Rae, T. C. and Koppe, T., 2004. Holes in the head: evolutionary interpretations of the paranasal sinuses in catarrhines. *Evolutionary Anthropology: Issues, News, and Reviews*, 13, 211-223.

Rae, T. C. and Koppe, T., 2008. Independence of biomechanical forces and craniofacial pneumatization in Cebus. *The Anatomical Record*, 291, 1414-1419.

Rae, T. C., and Koppe, T., 2014. Sinuses and flotation: Does the aquatic ape theory hold water? *Evolutionary Anthropology: Issues, News, and Reviews*, 23, 60-64.

Rae, T. C., Koppe, T., Spoor, F., Benefit, B. and McCrossin, M., 2002. Ancestral loss of the maxillary sinus in Old World monkeys and independent acquisition in *Macaca*. *American journal of physical anthropology*, 117, 293-296.

Rae, T. C., Koppe, T., and Stringer, C. B., 2011. The Neanderthal face is not cold adapted. *Journal of Human Evolution*, 60, 234-239.

Ritman, R. L., 2004. Micro-Computed Tomography—Current status and developments. *Annu. Rev. Biomed. Eng*, 6, 185–208.

Rook, L., Mottura, A. and Gentili, S., 2001. Fossil *Macaca* remains from RDB quarry (Villafranca d'Asti, Italy): new data and overview. *Journal of Human Evolution*, 40, 187-202.

Roseman, C. C., 2004. Detecting interregionally diversifying natural selection on modern human cranial form by using matched molecular and morphometric data. *Proceedings of the National Academy of Sciences of the United States of America*, USA, 101, 12824-12829.

Rossie, J. B., 2006. Ontogeny and homology of the paranasal sinuses in Platyrrhini (Mammalia: Primates). *Journal of Morphology*, 267, 1-40.

Rossie, J. B., Simons, E. L., Gauld, S. C., and Rasmussen, D. T., 2002. Paranasal sinus anatomy of *Aegyptopithecus*: implications for hominoid origins. *Proceedings of the National Academy of Science*, 99, 8454-8456.

Rowe, N., 1996. *Pictorial guide to the living primates.* Pogonias Press, 263 pages.

Schlosser, M., 1924. *Fossil Primates from China*. Paleontologia Sinica Series C, vol. I, fasc. 2, 1-18.

Shea, B. T., 1977. Eskimo craniofacial morphology, cold stress and the maxillary sinus. *American Journal of Physical Anthropology*, 47, 289-300.

Simons E. L., 1970. The development and history of Old World monkeys. In: Napier, J. R. and Napier, P. H. (eds) *Old World Monkeys*. Academic Press, New York, 97-137.

Simons, E. L., Seiffert, E. R., Ryan, T. M. and Attia, Y., 2007. A remarkable female cranium of the early Oligocene anthropoid *Aegyptopithecus zeuxis* (Catarrhini, Propliopithecidae). *Proceedings of the National Academy of Sciences*, 104, 8731-8736.

Singleton, M., 2002. Patterns of cranial shape variation in the Papionini (Primates: Cercopithecinae). *Journal of Human Evolution*, 42, 547-578.

Smith, S. W., 1999. *The Scientist and Engineer's Guide to Digital Signal Processing*. California Technical Publishing, 2nd Edition, 640 pages.

Smith, T. M., Tafforeau, P., Reid, D. J., Grun, R., Eggins, S., Boutakiout, M. and Hublin, J. J., 2007. Earliest evidence of modern human life history in North African early *Homo sapiens*. *Proceedings of the National Academy of Sciences*, 104, 6128-6133.

Springer, M. S., Meredith, R. W., Gatesy, J., Emerling, C. A., Park, J., Rabosky, D. L., Stadler, T., Steiner, C., Ryder, O. A., Janecka, J. E., Fisher, C. A., and Murphy, W. J., 2012. Macroevolutionary dynamics and historical biogeography of primate diversification inferred from a species supermatrix. *PloS one*, 7, e49521.

Stock, S. R., 2009. *MicroComputed tomography : methodology and applications*. CRC Press, 336 pages.

Strasser, E., and Delson, E., 1987. Cladistic analysis of cercopithecid relationships. *Journal of Human Evolution*, 16, 81-99.

Suwa, G., Kono, R. T., Katoh, S., Asfaw, B. and Beyene, Y., 2007. A new species of great ape from the late Miocene epoch in Ethiopia. *Nature* 448: 921-924.

Szalay, F. S. and Delson, E., 1979. *Evolutionary History of the Primates*. Academic Press, New York, 580 pages.

Takai, M., Maschenko, E. N., Nishimura, T. D., Anezaki, T. and Suzuki, T., 2008. Phylogenetic relationships and biogeographic history of *Paradolichopithecus sushkini* Trofimov 1977, a large-bodied cercopithecine monkey from the Pliocene of Eurasia. *Quaternary International*, 179, 108-119.

Takai, M., Zhang, Y., Kono, R. T. and Jin, Ch., 2014. Changes in the composition of the Pleistocene primate fauna in southern China. *Quaternary International*, 354, 75-85.

Ting, N., Harcourt-Smith, W. E. H., Frost, S. R., and Delson, E., 2004. Description and analysis of postcranial elements of *Paradolichopithecus arvernensis*: A large-bodied papionin from the Pliocene of Eurasia (abstract). *American Journal of Physical Anthropology*, Suppl. 38, 195.

Tosi, A. J., Morales, J. C., and Melnick, D. J., 2003. Paternal, maternal, and biparental molecular markers provide unique windows onto the evolutionary history of macaque monkeys. *Evolution*, 57, 1419-1435.

Trovimov, B.A., 1977. Primate *Paradolichopithecus sushkini* sp. nov. from the Upper Pliocene of the Pamir Piedmont. *Journal of the Palaeontological Society of India*, 20, 26-32.

Weiglein, A. H., 1999. Development of the paranasal sinuses in humans. In: Koppe, T., Nagai, H. and Alt, K.W. (eds.) *The Paranasal Sinuses of Higher Primates: Development, Function, and Evolution*. Quintessence, Berlin, 35-50.

Witmer, L. M., 1997. The evolution of the antorbital cavity of archosaurs: a study in softtissue reconstruction in the fossil record with an analysis of the function of pneumaticity. *Journal of Vertebrate* Paleontolog, 17 (S1),1-76.

Witmer, L. M., 1999. The phylogenetic history of paranasal air sinuses. In: Koppe, T., Nagai, H. and Alt, K.W. (eds.) *The Paranasal Sinuses of Higher Primates: Development, Function, and Evolution*. Quintessence, Berlin, 21-34.

Yokley, T. R., 2009. Ecogeographic Variation in Human Nasal Passages. *American journal of physical anthropology*, 138, 11-22.

Zollikofer, C. P. E. and Weissmann, J. D., 2008. A morphogenetic model of cranial pneumatization based on the invasive tissue hypothesis. *The Anatomical Record*, 291, 1446-1454.

Digital Morphology Museum (DMM), KUPRI, http://dmm3.pri.kyoto-u.ac.jp/dmm/WebGallery/index.html

Appendix

Tables

Table I. Specimens of the fossil genus of *Procynocephalus/Paradolichopithecus* from studied localities.

Species	Citation	Locality	Material	Age
P. arvernensis	Depéret, 1929	Senèze, France	the calvaria and face, left maxilla with I^1–^{2} and P^3-M^3, isolated left upper canine the muzzle with the right I_2 to M_3, isolated right I1, and the complete mandible with full dentition	Early Pleistocene
P. arvernensis	Heintz *et al*., 1974; Delson, 1973	Vialette, France	a molar ? (questioned by Lacombat *et al*., 2008)	Late Pleiocene
P. arvernensis	Heintz *et al*., 1971; Aguirre & Soto, 1978; Marigo *et al*., 2014	La Puebla de Valverde, Spain	an incomplete left hemimandibIe of an immature individual	Early Pleistocene
P. arvernensis	de Vos *et al*., 2002	Vatera, Greece	an upper premolar; an upper canine; one mandible I- M_2; Plate I, C; one mandible with I_1-M_3; a right humerus; a left humerus; a right ulna; a right radius; a left olecranon; four radious fragments; a distal right tibia; a right astragalus	Late Pleiocene
P. geticus	Necrasov *et al*., 1961; Bolomey, 1965	Valea Graunceanului, Romania	parts of eight crania or mandibles and postcranial (right, left humerus, right radius, right ulna)	Late Pleiocene
P. sushkini	Tofimov, 1977; Maschenko, 1994	Kuruksay, Tadjikistan	a cranium of an adult female; a facial skeleton of a subadult male	Late Pleiocene
P. gansuensis	Qiu *et al*., 2004	Longdan, Gansu, China	a nearly complete mandible lacking right M_3; a partial maxilla lacking right I^1–^{2}	Early Pleistocene
Pr. winami	Schlosser, 1924	Xin'an, Henan, China	a posterior part of right maxilla with M^2–^{3}; a posterior part of left maxilla with M^2–$_3$; an anterior part of the left upper jaw with a canine and P^3; an isolated left M1; a nearly complete mandible lacking the left	Late Pliocene/ Early Pleistocene

			M_3	
Pr. subhimalayanus	von Meyer, 1848	Upper Siwaliks, India	fragment of right maxilla of a female and P^1-M^3	Late Pliocene/ Early Pleistocene
Procynocephalus/ *Paradolichopithecus* aff. *arvernensis* DFN3-150	Kostopoulos *et al*., *submitted*	Dafnero-3, Greece	cranium lacking incisors and canine	Early Pleistocene

Table II. Results of the independent t-test among the two extant genera using all the metrical data. Highlighted (in bold) are the values showing high significance correlation between *Papio* and *Macaca* for each measurement.

		Levene's Test for Equality of Variances		t-test for Equality of Means						
		F	Sig.	t	df	Sig. (2-tailed)	Mean Difference	Std. Error Difference	95% Confidence Interval of the Difference	
									Lower	Upper
ba_n	Equal variances assumed	.224	.641	-4.769	22	.000	-.0772	.0162	-.1108	-.0436
	Equal variances not assumed			-4.737	20.704	.000	-.0772	.0163	-.1112	-.0433
i_pr	Equal variances assumed	2.312	.143	-8.162	22	.000	-.1708	.0209	-.2142	-.1274
	Equal variances not assumed			-8.026	19.418	.000	-.1708	.0212	-.2153	-.1263
i_n	Equal variances assumed	1.324	.262	-6.201	22	.000	-.0920	.0148	-.1228	-.0612
	Equal variances not assumed			-6.146	20.432	.000	-.0920	.0149	-.1233	-.0608
ba_pr	Equal variances assumed	3.189	.088	-7.173	22	.000	-.1701	.0237	-.2193	-.1209
	Equal variances not assumed			-7.022	18.797	.000	-.1701	.0242	-.2208	-.1193
ba_sta	Equal variances assumed	.353	.558	-5.761	22	.000	-.1307	.0227	-.1778	-.0837
	Equal variances not assumed			-5.700	20.237	.000	-.1307	.0229	-.1786	-.0829
ba_b	Equal variances assumed	.400	.534	-5.068	22	.000	-.0710	.0140	-.1001	-.0419
	Equal variances not assumed			-5.050	21.022	.000	-.0710	.0140	-.1003	-.0418
pr_n	Equal variances assumed	.020	.888	-9.232	22	.000	-.2676	.0289	-.3277	-.2075
	Equal variances not assumed			-9.243	21.442	.000	-.2676	.0289	-.3278	-.2075

po_po	Equal variances assumed	.202	.657	-4.634	22	.000	-.1045	.0225	-.1513	-.0577
	Equal variances not assumed			-4.629	21.266	.000	-.1045	.0225	-.1514	-.0576
FM_width	Equal variances assumed	.399	.534	-6.375	22	.000	-.0981	.0153	-.1300	-.0662
	Equal variances not assumed			-6.554	21.517	.000	-.0981	.0149	-.1292	-.0670
FM_length	Equal variances assumed	.481	.495	-4.835	22	.000	-.1143	.0236	-.1633	-.0653
	Equal variances not assumed			-4.949	21.791	.000	-.1143	.0231	-.1622	-.0664
o_sta	Equal variances assumed	1.780	.196	-6.218	22	.000	-.1196	.0192	-.1595	-.0797
	Equal variances not assumed			-6.368	21.767	.000	-.1196	.0187	-.1586	-.0806
pr_po	Equal variances assumed	.874	.360	-6.443	22	.000	-.1594	.0247	-.2107	-.1081
	Equal variances not assumed			-6.310	18.859	.000	-.1594	.0252	-.2123	-.1065
po_n	Equal variances assumed	.044	.835	-4.866	22	.000	-.0875	.0179	-.1247	-.0502
	Equal variances not assumed			-4.858	21.201	.000	-.0875	.0180	-.1249	-.0500
sta_pr	Equal variances assumed	2.092	.162	-7.694	22	.000	-.2008	.0261	-.2550	-.1467
	Equal variances not assumed			-7.533	18.801	.000	-.2008	.0266	-.2567	-.1450
Prem_Cani	Equal variances assumed	1.012	.325	-4.905	22	.000	-.1204	.0245	-.1714	-.0695
	Equal variances not assumed			-4.847	20.094	.000	-.1204	.02485	-.1723	-.0686
M1_M2	Equal variances assumed	1.515	.231	-6.738	22	.000	-.1119	.0166	-.1463	-.0774
	Equal variances not assumed			-6.590	18.643	.000	-.1119	.0169	-.1475	-.0763
M3_mid	Equal variances assumed	2.598	.121	-5.804	22	.000	-.1163	.0200	-.1578	-.0747
	Equal variances not assumed			-5.543	15.074	.000	-.1163	.0209	-.1610	-.0716
n_ns	Equal variances assumed	.001	.982	-9.731	22	.000	-.2857	.0293	-.3465	-.2248
	Equal variances not assumed			-9.687	20.929	.000	-.2857	.0294	-.3470	-.2243
n_rhi	Equal variances assumed	.260	.615	-8.918	22	.000	-.3329	.0373	-.4104	-.2555
	Equal variances not assumed			-8.791	19.761	.000	-.3329	.0378	-.4120	-.2539
fmt_fmt	Equal variances assumed	.010	.921	-3.384	22	.003	-.0682	.0201	-.1100	-.0264

	Equal variances not assumed			-3.417	21.915	.002	-.0682	.0199	-.1096	-.0268
pt_pt	Equal variances assumed	.015	.905	-5.728	22	.000	-.0861	.0150	-.1173	-.0549
	Equal variances not assumed			-5.762	21.745	.000	-.0861	.0149	-.1172	-.0551
po_g	Equal variances assumed	.663	.424	-4.925	22	.000	-.0894	.0181	-.1270	-.0517
	Equal variances not assumed			-4.896	20.777	.000	-.0894	.0182	-.1274	-.0514
Orbits_width	Equal variances assumed	.763	.392	-3.762	22	.001	-.0488	.0129	-.0758	-.0219
	Equal variances not assumed			-3.938	19.307	.001	-.0488	.0124	-.0748	-.0229
Orbits_height	Equal variances assumed	.007	.936	-1.871	22	**.075**	-.0232	.0124	-.0489	.0025
	Equal variances not assumed			-1.871	21.358	**.075**	-.0232	.0124	-.0490	.0025
o_i	Equal variances assumed	2.153	.156	-4.815	22	.000	-.1462	.0303	-.2091	-.0832
	Equal variances not assumed			-4.710	18.673	.000	-.1462	.0310	-.2112	-.0811
b_i	Equal variances assumed	.189	.668	-4.483	22	.000	-.0751	.0167	-.1099	-.0403
	Equal variances not assumed			-4.427	19.984	.000	-.0751	.0169	-.1105	-.0397
b_o	Equal variances assumed	.415	.526	-4.549	22	.000	-.0703	.0154	-.1024	-.0382
	Equal variances not assumed			-4.666	21.673	.000	-.0703	.0150	-.1016	-.0390
Carotid_Foramen_distance	Equal variances assumed	.440	.514	-4.867	22	.000	-.0877	.0180	-.1251	-.0503
	Equal variances not assumed			-5.003	21.519	.000	-.0877	.0175	-.1241	-.0513
Frank_o_i	Equal variances assumed	.015	.902	.116	22	**.909**	.0036	.0312	-.0610	.0683
	Equal variances not assumed			.115	20.374	**.910**	.0036	.0315	-.0620	.0692
Frank_orbital_plane	Equal variances assumed	.260	.615	1.919	22	**.068**	.0211	.0109	-.0017	.0439
	Equal variances not assumed			1.944	21.984	**.065**	.0211	.0108	-.0014	.0436
Flower_Angle	Equal variances assumed	.093	.763	-5.794	22	.000	-.1112	.0192	-.1510	-.0714
	Equal variances not assumed			-5.776	21.075	.000	-.1112	.0192	-.1513	-.0712
ba_rhi_ba_n	Equal variances assumed	.068	.796	-7.801	22	.000	-.2099	.0269	-.2658	-.1541
	Equal variances not assumed			-7.829	21.612	.000	-.2099	.0268	-.2656	-.1543

Table III. Loadings of the PC1 and PC2 for each of the 29 measurements used in the PCA. The most important variables are highlighted.

Measurements	PC1	PC2
Basicranial length	+0.1116	+0.1386
Skull length	+0.216	+0.1164
Cranial length	+0.1225	+0.1276
Facial length	+0.2203	+0.1508
Cranial base length	+0.1707	+0.2148
Cranial height	+0.0909	+0.0340
Upper Facial height	**+0.3289**	-0.114
Biporionic breadth	+0.1454	**+0.2216**
Foramen Magnum maximum width	+0.1165	-0.012
Foramen Magnum maximum length	+0.1299	-0.213
Position Foramen Magnum end	+0.1568	+0.1061
Prosthion placement	+0.2052	-0.0119
Nasion placement	+0.1278	+0.1245
Palatal length	+0.2563	+0.0981
Bicanine breadth	+0.1624	+0.2166
Bimolar breadth	+0.138	+0.0281
Middle M^3 breadth	+0.1523	+0.1138
Nasal height	**+0.348**	-0.1276
Nasal length	**+0.4061**	**-0.2755**
Biorbital breadth	+0.1088	+0.1856
Postorbital min breadth	+0.0997	+0.0211
Glabela placement	+0.1286	+0.1574
Average Orbits width	+0.0672	+0.0534
Inion placement	+0.198 (o-i) +0.0854 (b-i)	**+0.3627** +0.007
Bregma placement	+0.0887	+0.0272
Distance between Carotid Canal of Foramen	+0.1017	-0.1122
Flower Angle	+0.1228	**-0.3434**
Middle Muzzle Angle	+0.2327	**-0.5069**

Figures

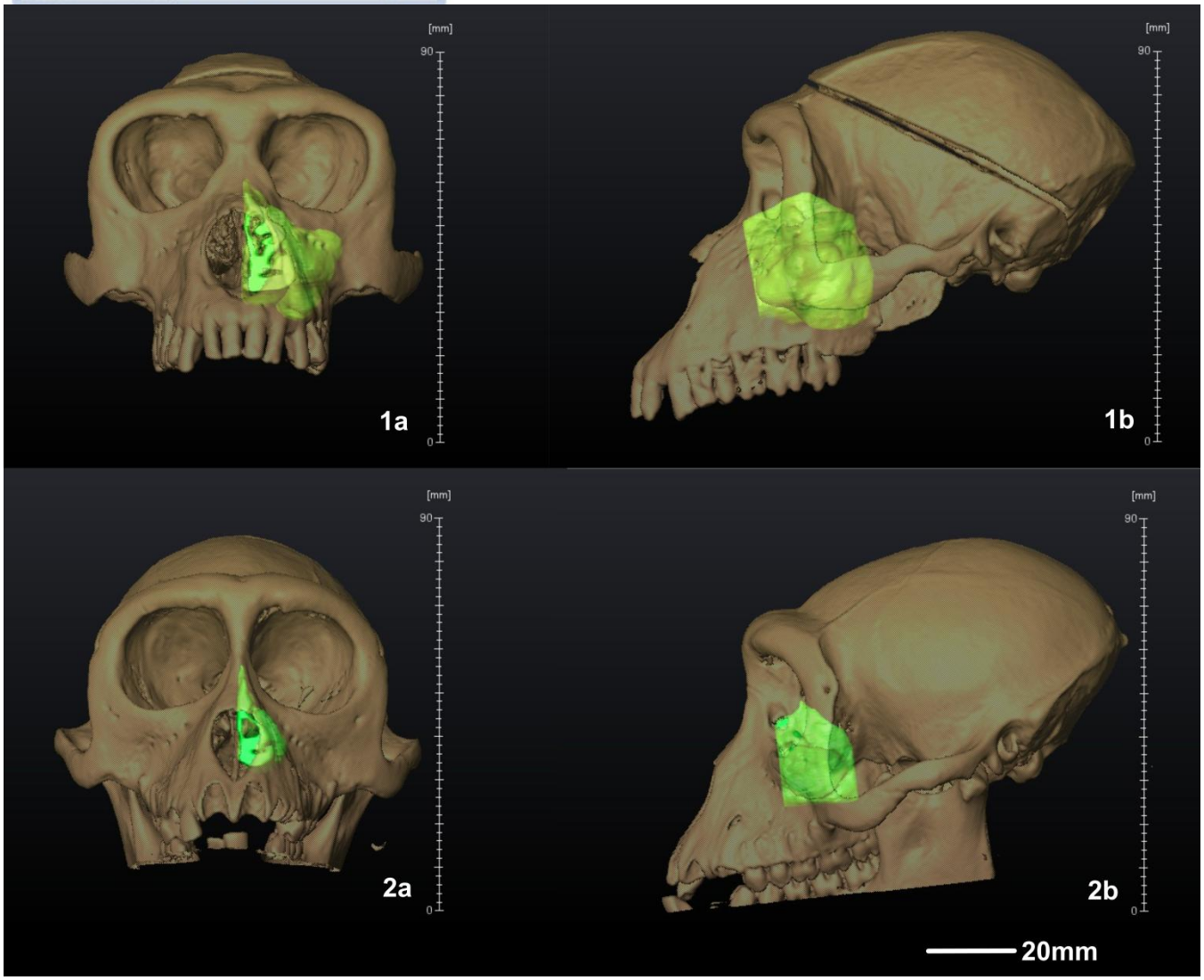

Figure I: Three-dimensional reconstruction of maxillary sinus and half nasal cavity (green color) with transparent facial cranium of the specimens *M. sylvanus* 1136KUPRI at the norma frontalis (1a) and norma lateralis-sinistra (1b) and *M.silenus* 38KUPRI (2a, 2b). Images done in Avizo software.

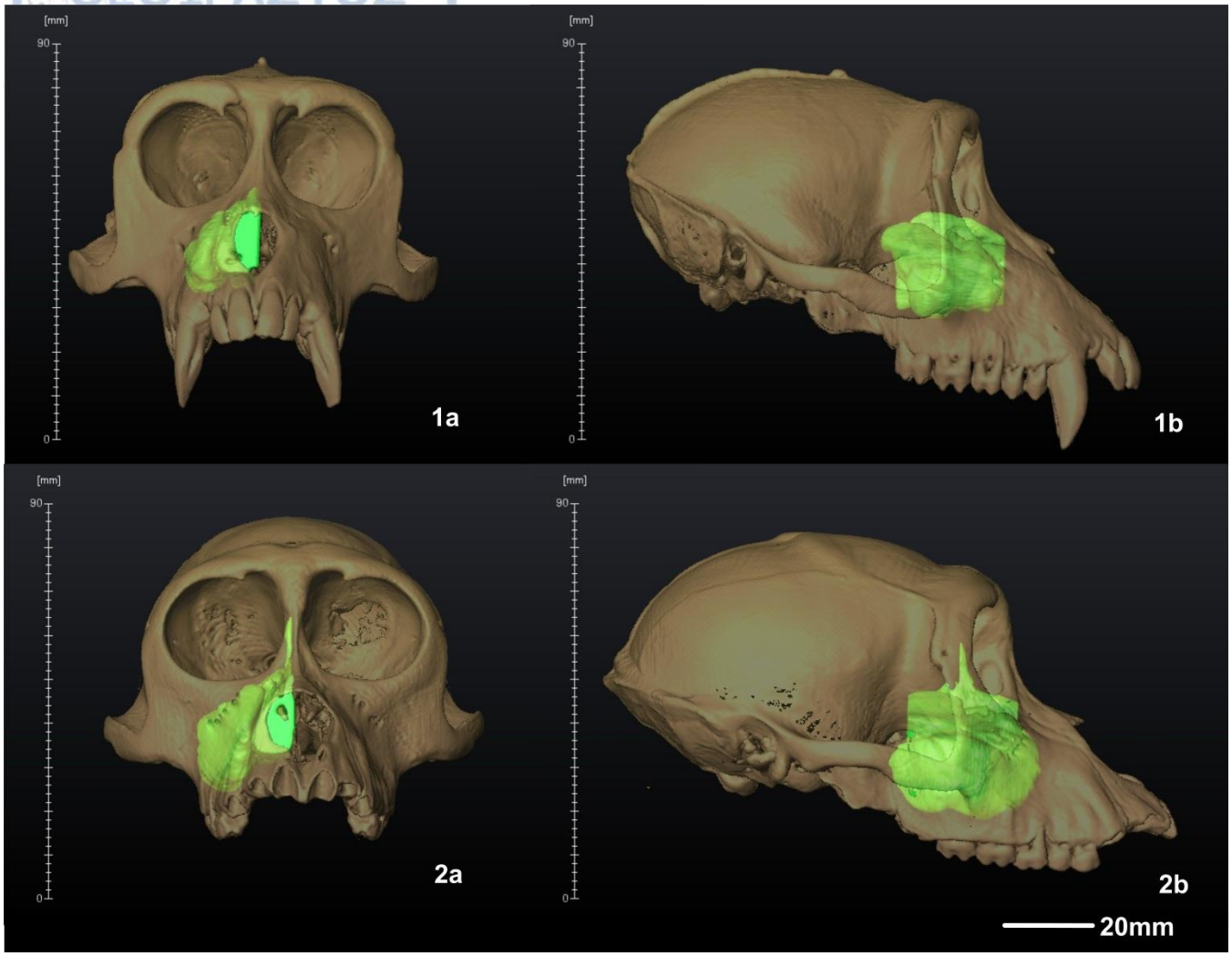

Figure II: Three-dimensional reconstruction of maxillary sinus and half nasal cavity (green color) with transparent facial cranium of the specimens *M. fascicularis* 1157KUPRI at the norma frontalis (1a) and norma lateralis-sinistra (1b) and *M.nemestrina* 1470KUPRI (2a, 2b), processed in Avizo software.

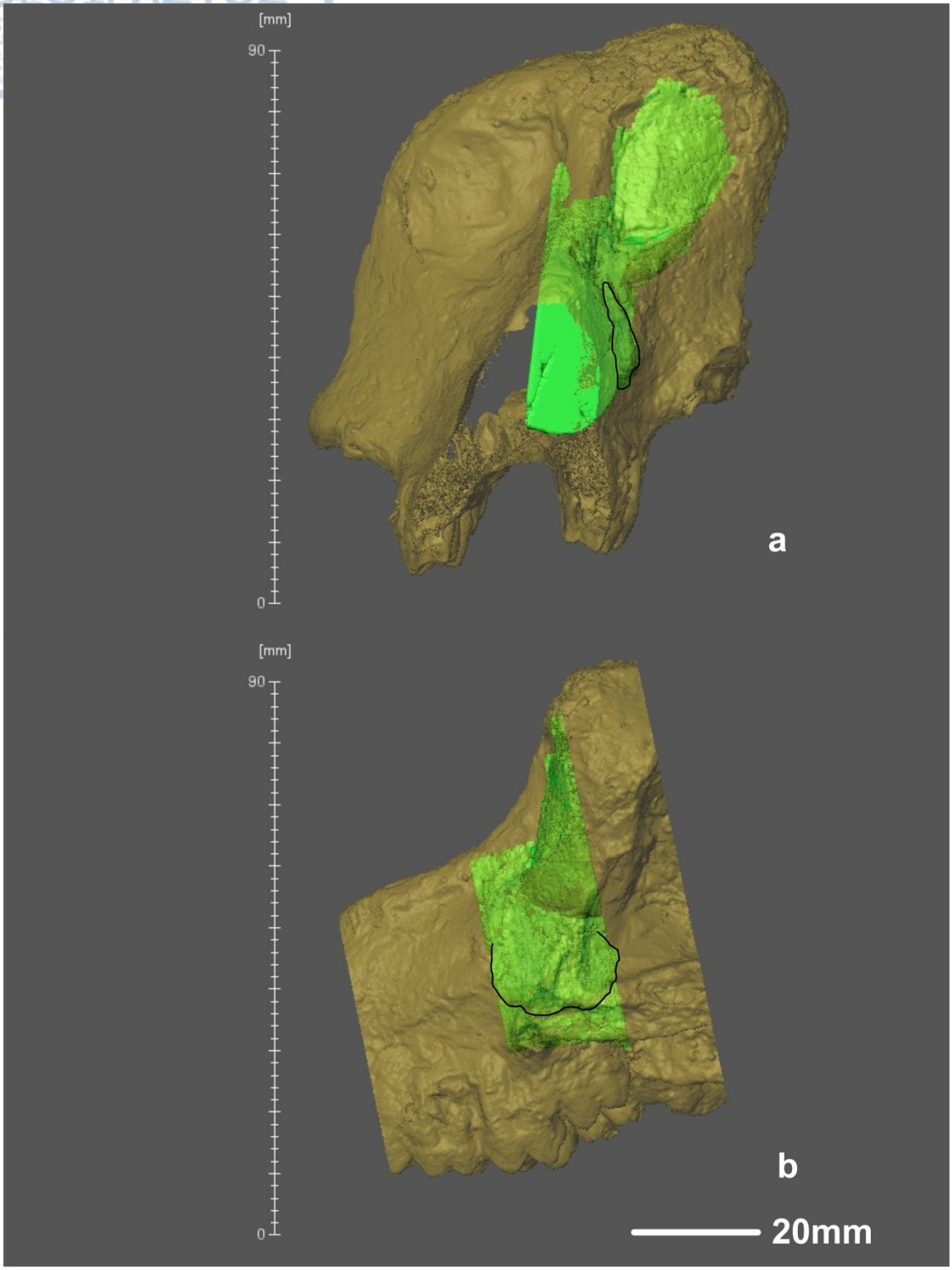

Figure III: Three-dimensional reconstruction of maxillary sinus, half nasal cavity and the orbital cavity (green color) with transparent part of the facial cranium of DFN3-150. The images are from the Avizo software and the margins of the MS were highlighted (black line) in Surfer software.

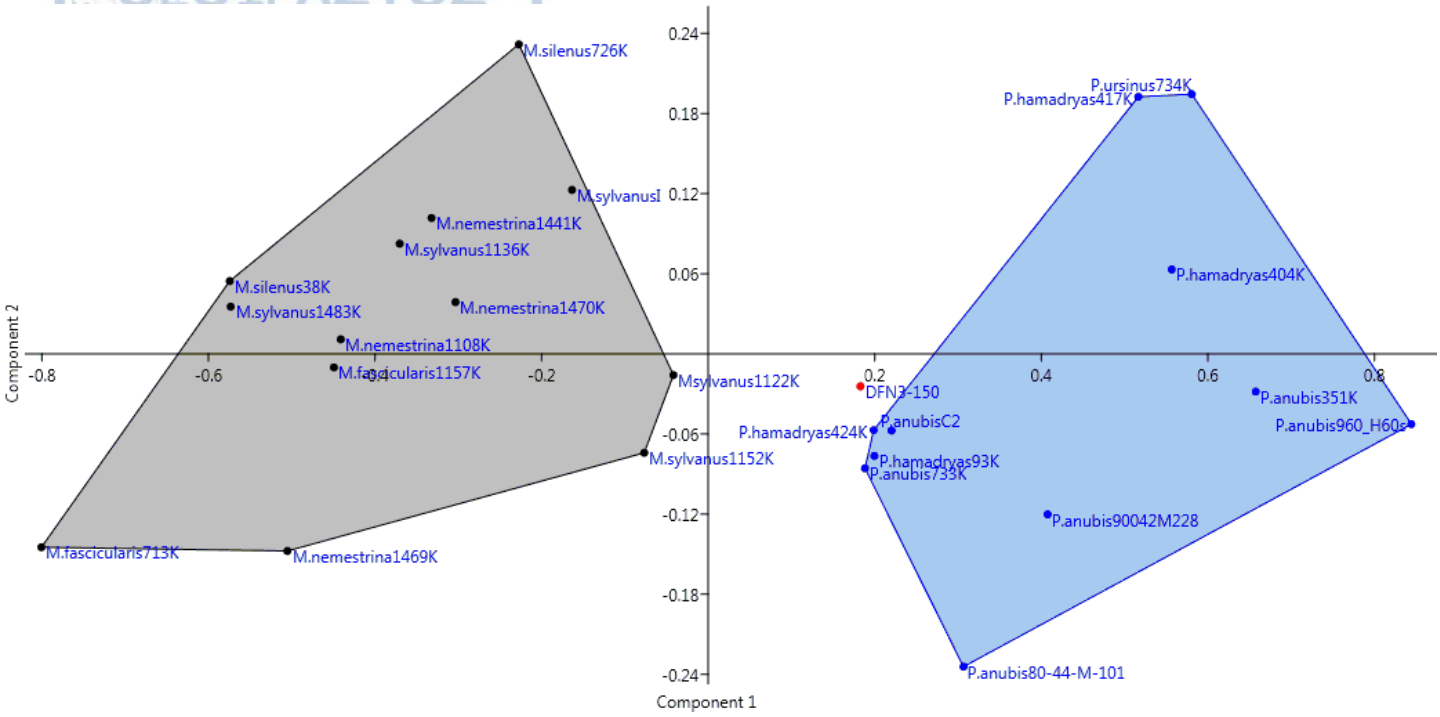

Figure IV. Scatter plot of the PCA using all the data of the external measurements and the estimated convex hull polygon.

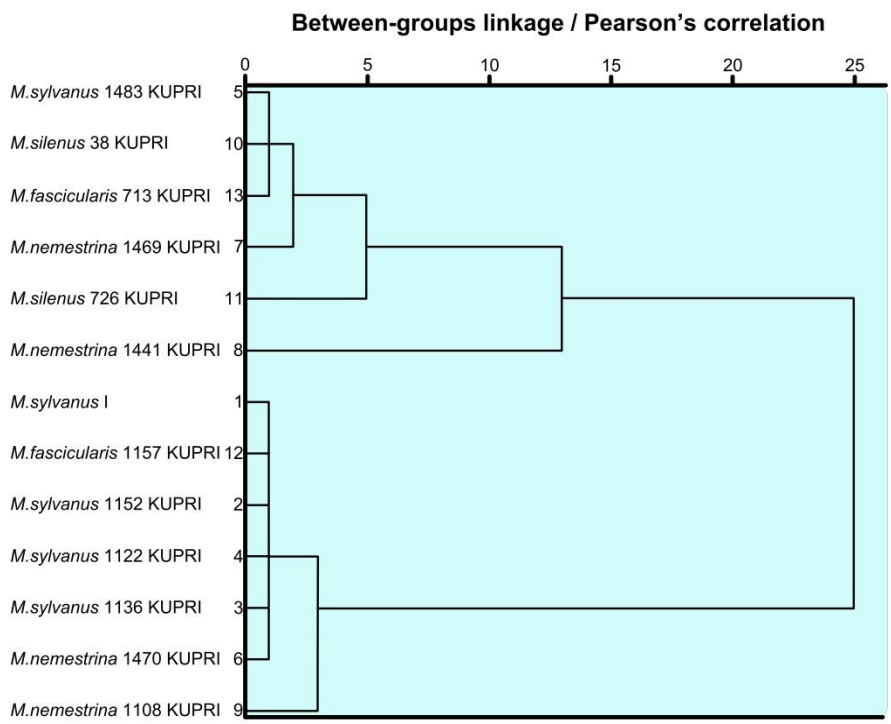

Figure V. Dendrogram of hierarchical BGL-PC cluster analysis for the maxillary sinuses' dimensions of the *Macaca* species.

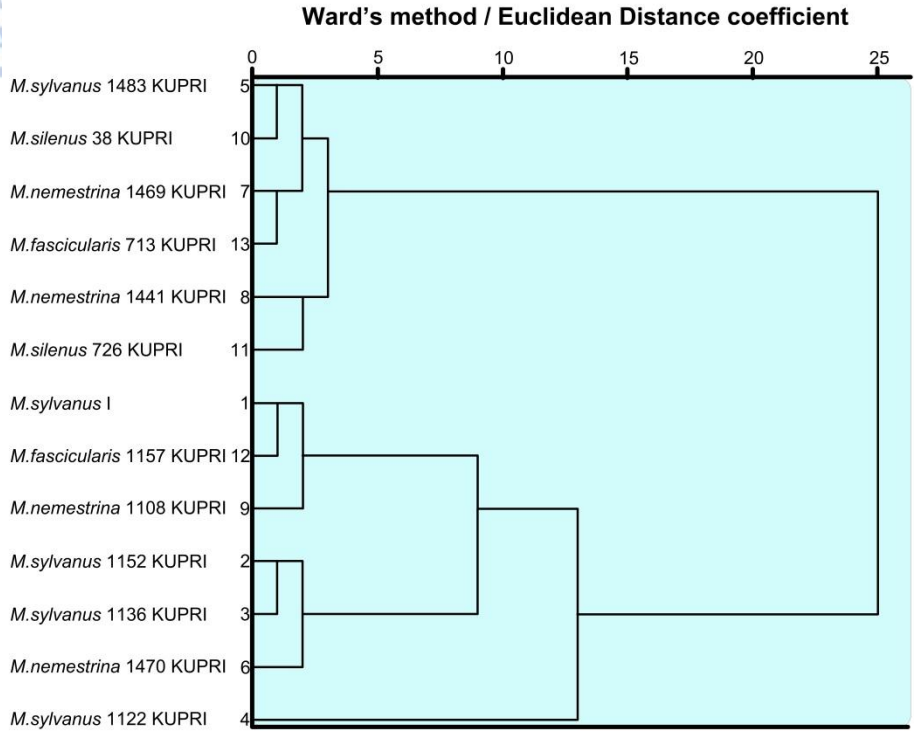

Figure VI. Dendrogram of hierarchical WM-ED cluster analysis using the maxillary sinuses' dimensions of the extant *Macaca* species.